# NOVEL CONCENTRATED-LIGHT AGING TECHNIQUES FOR HIGH-TEMPERATURE AND SOLAR-ENERGY MATERIALS

A Thesis

by

BASSAM KHALIL

Submitted to the Office of Graduate and Professional Studies of
Texas A&M University
in partial fulfillment of the requirements for the degree of

MASTER OF SCIENCE

| | |
|---|---|
| Chair of Committee, | Konstatinos Kakosimos |
| Committee Members, | Mohammed Al-Hashimi |
| | Ahmed Abdala |
| Head of Department, | Arul Jayaraman |

May 2020

Major Subject: Chemical Engineering

# ABSTRACT

Many materials have been synthesized in recent years to provide solutions to the ever so increasing demands of industrial processes, eco-friendly buildings, and optimization of renewable energy systems. During the recent years, significant engineering tests for solar energy products and materials have been developed, however, there is still a deficiency in the understanding and testing when it comes to the degradation effects driven by the combined effect of solar light intensity and exposure duration. Most of the methods developed neglect the need to test small quantities of materials or prototype devices that might operate at close to ambient conditions and need to demonstrate >25 years stability, while still being at the development stage and without the luxury to afford expensive and long (of weeks and months) tests. For example, the multitude of materials that are announced every day for photovoltaic applications, smart windows, and green buildings. The primary objectives of the research project were the development of a solar energy characterization facility and a methodology/apparatus for accelerated aging of materials based on concentrating light with continuous optical characterization and environmental control.

The deliverables were directly aimed to resolve the current deficiencies in the testing methodologies and included; the commissioning and flux characterization of a novel solar characterization facility along with an apparatus and methodology for accelerated aging of materials. Not only did the project deliverables provide an alternative to the current testing procedures, but they also were extremely cost and time-efficient. The

completion of the deliverables resulted in an invention which addresses the current technical limitations with testing procedures and offers both a methodology and an apparatus to investigate the light-induced degradation of research or commercial-grade materials by conducting efficiently accelerated aging tests under fully controlled conditions, while continuously collecting the light transmitted through the material to conduct continuous optical characterization. To protect the invention from being reverse engineered, a disclosure document has been submitted to protect the intellectual property (IP).

# ACKNOWLEDGEMENTS

I would like to thank my committee chair, Dr. Konstantinos Kakosimos, and my committee members, Dr. Ahmad Abdala and Dr. Mohammed Al-Hashimi, for their guidance and support throughout the course of this research.

I would also like to thank my friends and colleagues and the department faculty and staff for making my time at Texas A&M University a great experience. Finally, thanks to Family for their encouragement and continuous support throughout this endeavor.

# CONTRIBUTORS AND FUNDING SOURCES

This work was supervised by a thesis committee consisting of Professor Konstantinos Kakosimos (Chair) and Professors Mohammed Al-Hashimi and Ahmed Abdala of the Chemical Engineering Department at Texas A&M university at Qatar. All work for the thesis was completed independently by the student, under the advisement of Dr. Konstantinos Kakosimos.

This work was made possible by the financial support provided by office of research at Texas A&M University at Qatar by their research seed grants.

# NOMENCLATURE

| | |
|---|---|
| IEA | International Energy Agency |
| PV | Photovoltaic |
| OPV | Organic Photovoltaic |
| DC | Direct Current |
| GW | Gigawatt |
| AT | Accelerated Tests |
| EMMA | Equatorial mount with mirrors for accelerating |
| UAWS | Ultra-Accelerated Weathering System |
| UV | Ultraviolet |
| CSP | Concentrated Solar Power |
| Xe | Xenon |
| kW | Kilowatts |
| kW/m2 | Kilowatts per Meter squared |
| HFSS | High Flux Solar Simulator |
| UHFSS | Ultra High Flux Solar Simulator |
| P3HS | Poly (3-hexylselenophene) |
| P3HT | Poly (3-hexylthiophene) |

# TABLE OF CONTENTS

Page

# LIST OF FIGURES

Page

# LIST OF TABLES

Page

# 1. INTRODUCTION

Energy security has become an increasingly significant part of today's global economies and industries. As consumers and industries carry on to grow globally, so does the demand for more energy, in terms of fuels or electrical energy. Non-renewable fuels were, and are still an essential of meeting the current energy demands. Due to the surge in fossil fuel consumption, there has been an increase in the release of greenhouse gases which have caused global climate change, as illustrated in figure 1. This climate change can potentially lead to an increase in natural calamities globally, and due to their nature, energy obtained from hydrocarbons could not possibly last forever. The Paris Agreement, signed on November 2016 and by 146 countries [1], targets to control the pace of climate change by preventing an average global temperature rise to less than 2°C above pre-industrialized levels. International Energy Agency (IEA) estimates in its World Energy Outlook 2016 [2], renewable energy would account for 37% of power generation globally by 2040, which is an increase from 23% in 2016, to meet objectives of the Paris Agreement. The IEA also concludes that the pledges on their own would not be sufficient to curb the $CO_2$ emissions to the 2°C desired target, and would entail tougher policies and strategies to promote low carbon technologies. The most Common types of renewable energy include solar, wind, hydro and geothermal power.

Solar power is a predominantly worthwhile asset, given the abundant energy that could be obtained from the Sun. The two most common technologies for solar energy production are photovoltaic (PV), which transforms sunlight directly into DC electrical current, and solar thermal power plants, which use several mirrors to focus the thermal energy from the sun to a concentrator, which generates steam to power steam turbines for electrical generation. United Nations (UN) statistics until 2015, illustrate that the solar energy globally accounted for only ~0.86% of the total electricity generation [3], but in a broader spectrum, solar power sector has seen an considerable growth, rising from 6.4 GW in 2006 to 227 GW in 2015 [4], and its stake among other renewable energy sources is also growing, in 2016 alone an additional capacity of 70 GW solar power was added, which was a 32% increase from the previous year [5]. It is quite evident that the future for solar energy is very promising.

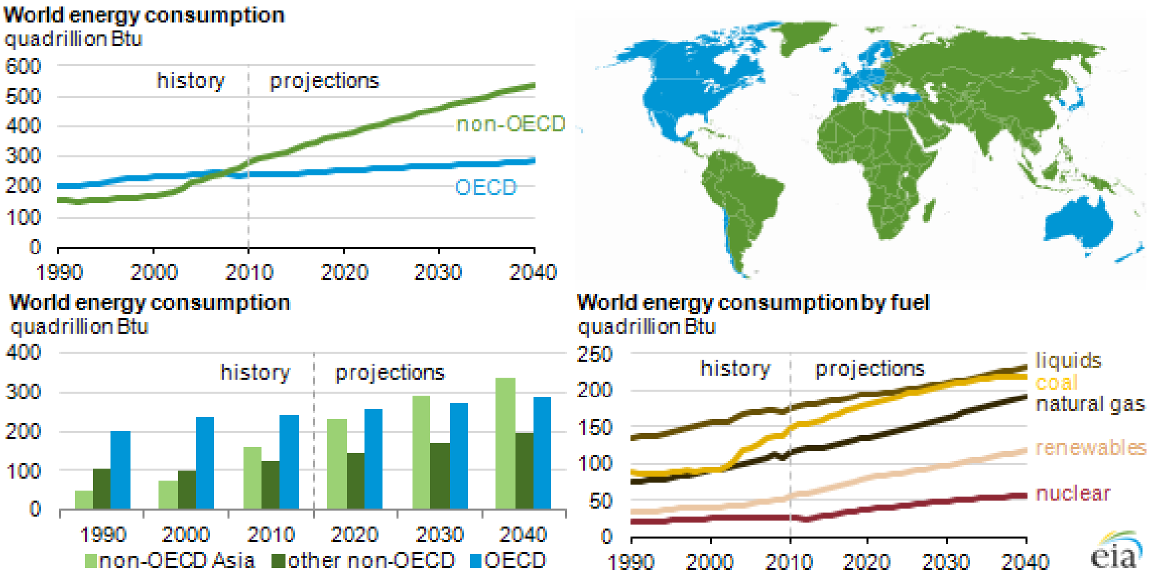

**Figure 1: Global energy demand by year 2040 by EIA, reprinted from [7].**

Many materials have been synthesized in recent years to provide solutions to the ever so increasing demands of industrial processes, eco-friendly buildings, and optimization of renewable energy systems [8]. Out of these developments, the solar energy sector has experienced the most advancement. Even though there are significant engineering tests, like thermal-stability and predicted lifetime for extreme temperature and solar energy products, there is still a deficiency of key parameters that one has to address [9]. For example, high-temperature rates and ultra-high concentrated heat flux for solar absorber material and photo-degradation for Organic Photovoltaic (OPV) modules. Data like this would give tremendous significant information regarding material design and construction, including flaws that help to identify any chance of a premature failure [10]. Conventional techniques are mostly used to assess new materials during the research and development phase, which is limited to conditions, such as low to moderate temperatures, humidity, and short testing time. Currently, the problem with these conventional testing methods is the scarcity in testing methodology for extreme temperature solar-energy materials, which is based on evaluating the materials performance and predicting its service life based on light-induced degradation [10].

## 1.1 Research objectives

The underlying deliverable of this research thesis is the development of a novel concentrated light aging facility and technique which would be effective to analyze the photo and thermal performance or stability of solar energy materials. A solar photo-thermal cell would be designed and manufactured, P3HT would be used as a base material to benchmark and test the initial methodology along with fullerene derivative blends to analyze the performance under different experimental conditions. The aforementioned methodologies would be utilized to carry out accelerated aging tests on novel OPV such as P3HS to study its characteristics. Four particular objectives will be carried out throughout the progression of this thesis;

1. Conduct flux characterization of a novel facility to analyze the thermal/photo-degradation of solar energy materials under well-regulated concentrated irradiance (up to 3000 times the irradiance from the sun)
2. Design, Fabrication, and testing of a solar photo-thermal cell that allows the standardized testing of solar materials under controlled experimental parameters including; Temperature, incident flux, ambient environment, humidity, etc.
3. Develop a standardized methodology to test materials under concentrated flux for accelerated aging and characterization of materials and extrapolate the results to predict the lifetime of the material under standard conditions using statistical models.
4. Benchmarking and testing of novel materials after the accelerated aging methodology is optimized and tested on a material of known degradation.

## 1.2 Motivation and need

Production of inorganic semiconductor materials is very expensive with regards to both the materials and the method. Over the years organic based photo voltaic cells are gaining interest due to their lower cost. However, they are not as efficient as the inorganic semiconductors due to their larger band gap. Furthermore, OPVs are very susceptible to water and oxygen. Intensive testing needs to be done to find a solution. The current testing methods have several short comings. Newly developed materials require comprehensive, fast and cost-efficient testing methods to provide proof of concept validation and initial stability and lifetime predictions. Table 1 illustrates the conventional aging techniques used currently and Figure 2 expands on the methods and the equipment used along with a cost evaluation.

**Table 1: Overview of the current testing methodologies**

| | Standard Outdoor Exposure | Conventional Standardised Lab Techniques | Novel Accelerated Aging Setups using concentrated light |
|---|---|---|---|
| **Cost** | Low | High | Medium- High |
| **Duration** | Weeks – Months | 1-2 Weeks | Hours - Day |
| **Limitations** | 1. Difficult to standardise due to geographical conditions.<br>2. Meteorological effects. | 1. Limited control over experimental parameters.<br>2. Low solar concentration ratios. | 1. Pre-treatment may be needed.<br>2. Experimental parameters neglected at high concentration ratios. |

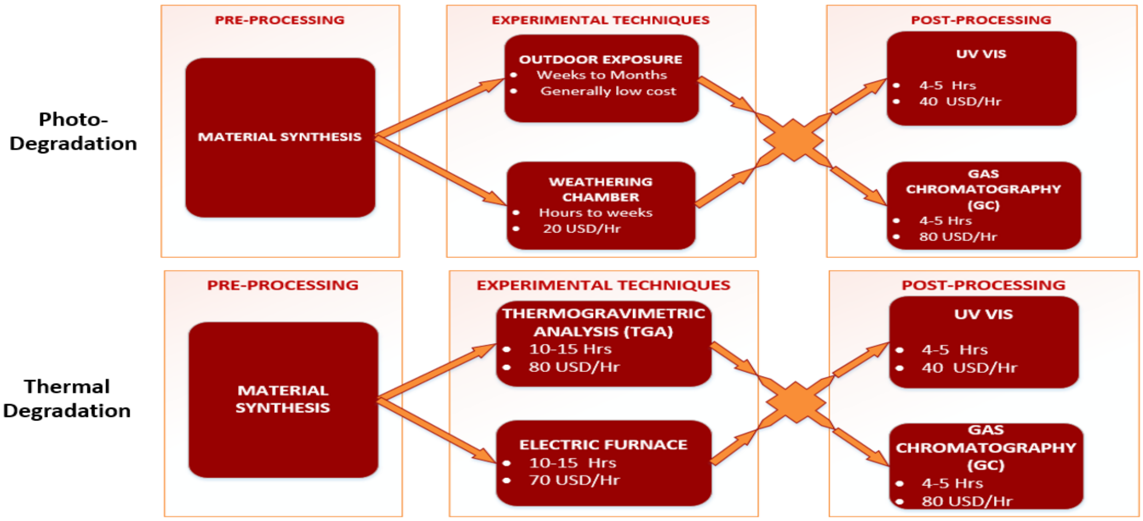

**Figure 2: Flowchart of current testing methods and equipment along with a preliminary cost breakdown**

# 2. LITERATURE REVIEW

Solar energy is one of the fastest growing renewable energy sources in recent years [6]. To be truly sustainable and have a low carbon footprint, it is absolutely necessary that the hardware components that make up these solar technologies are built to last long and they must maintain their optical characteristics, preferably for 25-30 years [9]. Thus, in the development phase of a new material, it has to go through rigorous durability testing. This testing includes performing an accelerated aging test on the material to simulate the degradation of its characteristics and also provide an estimate for its service life [8, 9]. These parameters can then be extrapolated in order to hypothesize the material's performance over time and under different service variables [11].

Aging is a process in which a material goes under thermal or photo-degradation and over time its performance and thermo-physical properties are measured [12]. Materials can be tested in a solar simulator for thermal or light-induced degradation, the solar simulator can be optimize to test both thermal and light-induced degradation at the same time using water-cooling techniques [13]. Accelerated aging is a process in which experiments are carried out on a material using high-stress parameters like temperature, humidity etc. Results obtained from these accelerated tests (AT) can then be fitted to a standard degradation mechanism to obtain the material's performance for its service life [14].

## 2.1 Current accelerated aging techniques

Accelerated testing for the aging of solar material has been around for nearly a century, carbon-arc was used as a substitute for sunlight for indoor testing and through the years, Xenon-arc has been used instead [15]. Previously, concentrated sunlight was used for the outdoor accelerated tests but none of these tests are time efficient and require extensive time constraints to be able to predict the weathering effects and the overall performance of the solar material. In 1980's EMMAQUA used concentrated sunlight for accelerated testing but it had a maximum acceleration rate of 10 and could predict 10-12 years of service life degradation in one year of testing [16]. Slow acceleration rates deter the use of new material in solar technology if it's in the preliminary stage of research and development.

Concentrated light has been used for outdoor Accelerated tests since 1980’ [15] in order to speed up the photo degradation by 5 to nearly 10 times, but higher acceleration rates were introduced only recently [17]. Organic photo-voltaic panels are particularly sensitive to light and mainly UV radiation, so they were one of the first materials to undergo tests using concentrated light; first up to 27 suns initially by Tromholt et al [18] and later on up to 10,000 suns by Katz et al. [19]. The acceleration rate of the experiment depends on the number of suns or the incident energy in watts per squared meters, but it not always linear or proportional. Lately, the collective effect of both high temperature and UV radiation, on Organic photo-voltaic materials was studied [18]. But, these studies were done using concentrated sunlight which limits the time and also the control over the incident radiation, because some of the observed variances could be associated to processes which happen in the dark periods [18]. With reference to other materials, Boubault et al [15] used concentrated homogenized sunlight to examine an accelerated test for Inconel 625 metal coated with Pyromark 2500 by adjusting only the incident radiation dosage and using low to medium concentration ratios. Cotfas et al. conducted an accelerated test for multiple PV cells (multijunction and monocrystalline) using un-homogenized concentrated synthetic light, therefore, there was poor control of the incident radiation [20]. In recent times, the group from TEXAS A&M Qatar conducted experiments to evaluate the thermal and optical properties of MAX phase ceramics using a well-regulated environment (including both UV radiation and temperature) using a homogenized artificial concentrated light source [21].

## 2.2 Ultra high flux solar simulator (UHFSS) and commercially used setups

To test materials and conduct solar energy research under realistic conditions, solar simulators are used. These solar simulators use one or multiple light sources and with the help of reflectors, they concentrate the light to a known focal point. It is really difficult to get homogenized and highly concentrated radiation and currently it relies heavily on visual analysis and the operator's experience. Figure 3 provides a comparison of the solar spectrum to the emission spectrum of Xe-Arc lamp, as measured in the lab at TAMUQ.

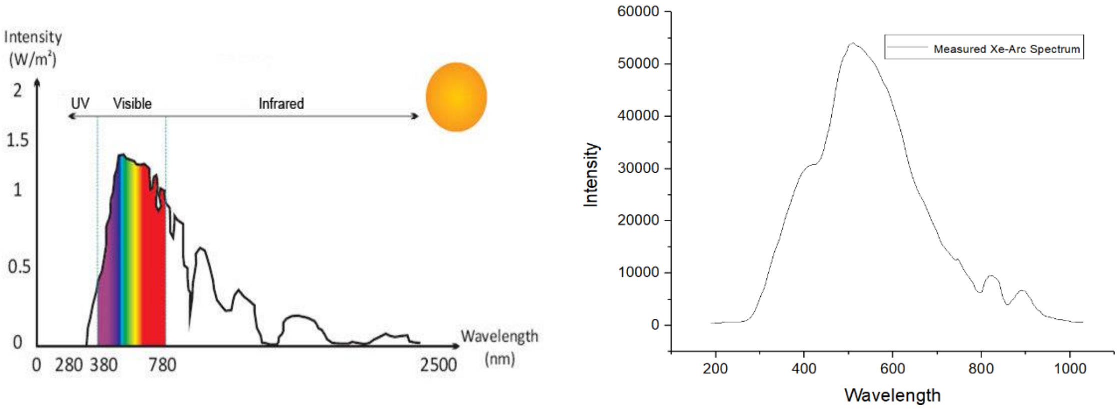

**Figure 3: Comparison of the emission spectrum of Xe-Arc lamp to the solar spectrum**

The ultra-high flux solar simulator (UHFSS) at the sustainable energy and clean air research lab at Texas A&M Qatar, uses seven Xenon-Arc Lamps with a combined power of 42 KWe. The facilty can be seen in figure 4. It can deliver a maximum power of 30 KWth with almost 70% efficiency, and the area of the focal point would be around 1-50 cm in radius. The maximum irradiance achieved from this setup can reach 3000 suns or 3000 kW/m2. Below are some of the current solar simulators commercially used in the industry;

**Figure 4: Outside and inside view of the new ultra high flux solar simulator (UHFSS) facility at TAMUQ.**

### 2.2.1 EMMA/EMMAQUA

Equatorial mount with mirrors for accelerating (EMMA) setup is a sunlight concentrator that works using the principle of Fresnel mirrors, developed by DSET lab in Arizona. The setup consists of flat mirror strips arranged symmetrically so that they focus the light on a thin rectangular receiver. The samples are placed on the receiver and they are kept at ambient temperature with the help of fans built-in to the receiver. The system is mounted on 2-axis controller so it can track the sun’s path. The EMMAQUA adds the option of spraying distilled water on the samples to simulate humidity. The radiation concentration factor is only 2-3 times the solar irradiance.

### 2.2.2 Ultra-accelerated EMMA

It uses a similar setup to EMMA but the difference is in the mirrors used for the setup, it uses special mirrors that reflect only UV and near visible IR spectrum. This helps to keep the sample cool while simultaneously increasing the effective radiation dosage. The concentration factor can go up to 5-10 times the solar irradiance depending on the setup.

### 2.2.3 Ultra-accelerated weathering system

UAWS is a sunlight concentrator capable of reaching concentration factors of 100 times the solar irradiance. The setup uses 29 of the special UV reflecting mirrors arranged in a way that it resembles a sphere with a 10-meter radius. Each of the mirrors can be individually adjusted and the whole setup is mounted on a metal frame with 2-axis control to track the suns' path. Each mirror is coated with 96 layers to only reflect the UV radiation responsible for photo degradation, the visible and near IR radiation which generates heat is impaired. The setup can generate a homogenized flux of 150*150mm at a focal distance of 5 meters. It uses a liquid coolant to cool down the sample in order to just analyze the effects of degradation by light.

### 2.2.4 Solar accelerated aging facility (SAAF)

SAAF is a sunlight concentrator made of several components and these components make it very convenient to control the irradiation concentration going to the target. The Unit uses heliostats similar to the ones used in CSP systems as depicted in figure 5. The heliostats reflect the solar radiation through a set of shutters to a parabolic concentrator. These shutters can be rotated amount of radiation going to the parabolic dish can be controlled pretty precisely. The parabolic dish; 2 meters in diameter, focuses the light on the sample receiver after going through a light collimator, which homogenizes the incident radiation. The receiver is liquid cooled and the setup can reach irradiances of 1500 suns over an area of 4cm2.

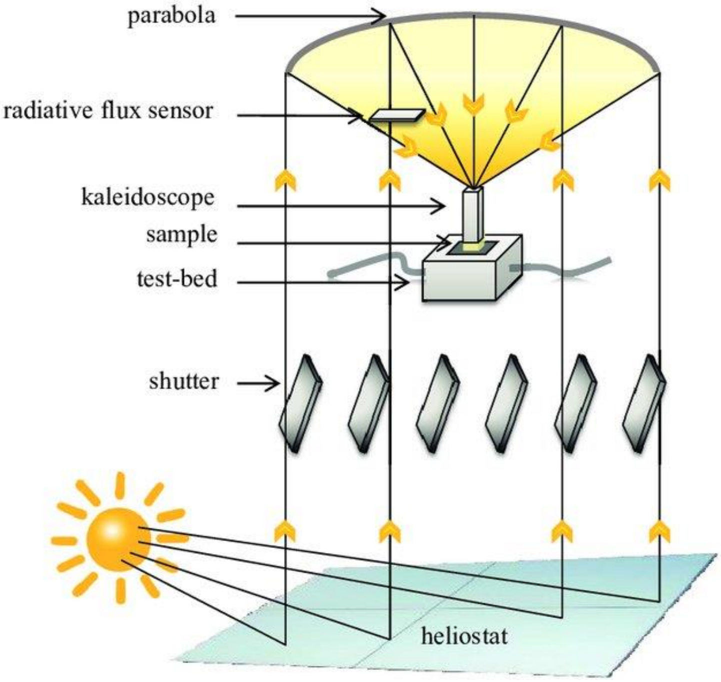

**Figure 5: Overview of the SAAF facility, reprinted from [14].**

### 2.2.5 DISTAL-1/Euro-dish

DISTAL-1 is a parabolic dish having a diameter of 7.5 meters. It's simple in construction and is equipped with a 3-axis movement controller. The sample is mounted in the focal point of the dish and it can either be water or air cooled. The unit can produce a peak flux of almost 6000 times the solar irradiance. The downside to this setup is the concentrated solar flux is not homogenized. An overview of the unit is shown in figure 6.

**Figure 6: Overview of the DISTAL-1/Euro-dish facility, reprinted from [22].**

### 2.3 Background literature for high flux solar simulators

A solar simulator is used to carry out accelerated weathering studies on a material by exposing it to extreme stresses like temperature, ultra violet radiation, humidity etc. The data from these accelerated aging tests are extrapolated using statistical models to predict the degradation of certain key parameters of that material in regular outdoor exposure [15]. These tests would require sunlight to be concentrated to increase the incident flux. However concentrating the radiation coming from the sun has proven to be unreliable because the weather conditions may vary and low energy density [21, 23]. An alternate to using natural solar radiation is use light sources in the laboratory that replicate the solar spectrum and can produce ultra-high levels of flux. Solar simulators generally use parabolic or ellipsoidal reflectors to concentrate light to a known focal plane and may comprise of multiple light sources [21]. The most common light sources is a Xe arc lamp because the emission spectrum that it produces resembles the solar spectrum [24]. Some other light sources may include incandescent, mercury vapor lamps, argon arc and metal halide lamps [25]. The use of solar simulators permits flexibility as the system does not rely on outdoor weather conditions. The flux generated by a solar simulator can be concentrated on a different surface area on the focal plane. The output can vary between 20 to 5000 kW/m2 [21].

Paul Scherrer Institute in Switzerland designed and built a 10 lamp HFSS, one of the first in the world, with the objective of maximizing the amount of radiant energy transferred to the target plane. The system provided a flux 6.8 MW/m2 [26]. Researchers in Australian National University (ANU) and Ecole Polytechnique Fédérale de Lausanne (EPFL) constructed a 45kW 18 lam HFSS whose experimental and numerical characterization method was documented by Leveque et al. Radiative flux maps were created by obtaining raw images of the target using a CCD camera which were then corrected for dark current, normalized y exposure time and calibrated with heat flux measurements. The measured peak flux was approximately 21.7 MW/m2 for the 18 lamp array. A 4.2% difference was found between the measured flux and the numerical results obtained using Monte-Carlo ray tracing software [26]. The lamp efficiency was found to be of 39.4%. Lastly, an adjustable flux solar simulator was developed and characterized by Jawad et al. in Texas A&M University at Qatar. The light source used was a 7kW xenon short arc lamp coupled with a truncated ellipsoid reflector. The performance of the HFSS was evaluated using the flux mapping method with the help of a CCD camera and a heat flux gage. A peak flux of 3.583 MW/m2 was reported at an input current of 153 A with conversion efficiency of 47%. Furthermore, the simulator was reported to be capable of adjusting its peak flux in the range of 2.074-3.583 MW/m2 [21]. A list of several other multi-lamp HFSSs is shown in Table 2 below.

**Table 2: Summary of HFSS around the world, adapted from [23].**

| Developer | Radiative Power (kW) | Efficiency | No. of lamps | Peak Flux ($kW/m^2$) | Target (mm) |
|---|---|---|---|---|---|
| Niigata University (TIT) | 133 | 25.0% | 19 | >3000 | 200 (Dia) |
| DLR | 21 | 33.3% | 10 | N.A. | 100 $cm^2$ |
| Minnesota University | 9.2 | 20.2% | 7 | 7300 | 60 (Dia) |
| GIT | 6 | 14.3% | 7 | >6500 | 40 (Dia) |
| IET | 6.4 | 22.9% | 4 | N.A. | 300 (Dia) |
| KTH | 19.7 * | 23.4% | 12 | 6730* | 200 (Dia) |
| Swinburne University | 12 | 28.6% | 7 | 927 | 175 (Dia) |
| JFCC | 8 | 10.7% | 20 | 37.7 | 4000x70 |
| Synlight | 320 | N.A. | 149 | 11000 | 200x200 |

*Ray Tracing Estimations

A high flux solar simulator cannot be commissioned and be used for research unless, the output incident flux is characterized. The key parameters that need to be characterized are the flux density distribution along with peak flux output [27]. A common method to determine these parameters is flux mapping. Flux mapping includes correlating the pixel values of images captured by a CCD camera to the flux readings taken from a heat flux gage. A lambertian target is used to reflect the incident flux and an image is captured by a CCD camera. The actual heat flux values are measured using a heat flux gage. A characterization curve is obtained when the pixel value of the image is correlated to the actual flux readings [28]. The characterization of the UHFSS at Texas A&M University at Qatar was done using the flux mapping method.

A considerable challenge with the UHFSS is obtaining the desired peak flux on a specific area distribution by adjusting the lamp position of multiple lamps simultaneously. Each of the lamps in the UHFSS has three degrees of freedom which can be controlled in the X, Y and Z axis using LabVIEW. Henceforth, the manual control and optimization of the individual lamps can be tedious and time consuming. An alternative suggestion for future research is incorporating convolutional neural networks (CNN) or machine learning to develop a statistical model which relates the individual lamp position to the output incident flux and the distribution on the target.

### 2.4 Organic photovoltaics

Conjugated polymer:fullerene blend films offer a low cost alternative for the formation of organic photovoltaic cells [29]. Of such conjugated polymers, poly(3-hexylthiophene) (P3HT) is the most well-known and studied organic material due to its excellent charge carrier mobility and long wave length absorption [30]. Studies have shown that blends of P3HT with fullerene derivatives have shown high efficiencies in comparison to other films [30]. P3HT is a semi-conductive organic photovoltaic (OPV) polymer that consists of a 3-phenylthiophene monomers. It is a semiconducting material that is used in a wide range of electronic applications especially in solar energy and batteries [31]. It has been well researched due to its low cost of production, simplicity and control of its production, and its availability [32]. P3HT is considered to be one of the most studied semiconducting molecules in both amorphous and crystalline structure. The polymer has unfavorable physical properties and is often further processed and improved such as doping it with fullerene for increased flexibility and lighter weight

P3HT is an important of its excellent electrical conductivity, electroluminescence, and nonlinear optical properties. However, its physical, thermal, and mechanical properties are poor and hinders its durability in many applications [31]. Its optoelectronic properties include high mobility, good chemical stability and low optical band gap. Technologically the polymer/fullerene blends offer the advantages of low cost technologies, lightweight and flexible substrates deposition [32].

In order to achieve greater efficiencies, a large part of the solar spectrum must be covered. Photovoltaic efficiency can be further improved by the development of polythiophene analogues that can capture more of the photo flux from the solar spectrum [30]. Poly(3-hexylselenophene) (P3HS) is an analogous polymer to poly(3-hexylthiophene) P3HT. It is formed by replacing the sulfur atom in the thiophene ring with selenium atom. Synthesis of P3HS can be done by electrochemical polymerization, oxidative polymerization, and Grignard-metathesis polymerization. In comparison to polythiophenes, polyselenophenes have lower oxidation and reduction potentials and better inter-chain transfer [33]. It was found that the relatively small difference in electronegativity of sulfur and selenium (2.5 for sulfur and 2.4 for selenium) resulted in both P3HS and P3HT having similar highest occupied molecular orbital (HOMO) energy levels [34]. Heeney et al. determined the band gap of P3HS to be 1.6eV compared to 1.9eV of P3HT indicating that P3HS absorbs at longer wavelengths than P3HT [32]. The gap between the conjugated polymer and the fullerene HOMO energy is proportional to the

$V_{oc}$ of the cells. Therefore, since the HOMO energy level of P3HS is like that of P3HT, P3HS absorbs at longer wavelengths than P3HT without compromising the open circuit voltage of the device. Furthermore, P3HS was exhibited better photo-stability compared to P3HT [29]. Chemical structures for both are given in figure 7.

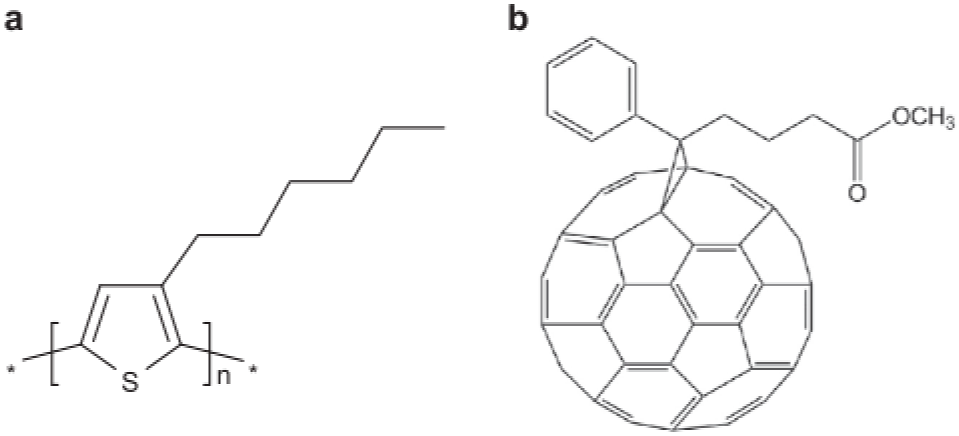

**Figure 7: Chemical structures of a) P3HT and b) PCBM- C61**

### 2.4.1 Photo-thermal degradation of organic photovoltaics

Hrostea *et al* discusses the effect of blending P3HT with PCBM in its Transmittance and morphology. The paper states that the transmittance is influenced by the amount of fullerene, such that in the infrared spectral range, the transmittance decreases considerably by in increasing the amount of fullerene; however, in the visible spectral range it is completely opposite as the transmittance gets improved by increase in amount of PCBM [35]. Rodrigues et al. carried out thermal stability analysis of P3HT in a molten state. P3HT samples were exposed to temperatures above 250$^{o}$ C and their properties were analyzed using a thermogravimetric analysis (TGA), NMR, FTIR-ATR etc. The study found that P3HT degrades rapidly under air atmosphere in a liquid state but degradation is not as noticeable under inert atmosphere. Another important conclusion was that the addition of PCBM slowed down the degradation process in both the high and low temperature conditions [36].

Tromholt et al. report the effects on organic photovoltaics of concentrated light. The study was conducted using concentrating the outdoor sunlight to a maximum concentration of 27 suns on a 1 cm2 area and looked at the power conversion efficiencies of bulk-heterojunction cells of P3HT-PCBM. [18]

### 2.5 Standardized photo-degradation models

Materials exposed to different stress factors like ultra violet (UV) radiation, temperature, humidity etc. degrade and that process is known as weathering. These stresses can contribute individually or as a combination to reduce a certain critical property of the material, after which the material is said to have reached the end of its life or has failed. For polymeric materials specifically, solar ultra violet (UV) radiation plays a critical role in weathering especially in the presence of humidity and temperature [37]. Extrapolating accelerated UV flux experiments have been conducted in the medical and biological fields over previous 100 years but it only started becoming relevant to the material industry after the 1960s [38]. Laboratory Ultra-high flux testing on materials has only recently been employed, as it was previously thought that the spectral emissions from indoor light sources did not replicate the solar spectrum and that exposure to ultra high radiation may cause the material to degrade in an unnatural mechanism which would be different from outdoor exposure [39].

Photo-degradation experiments require a generalization to predict the total degradation time in response to the exposure. According to Escobar & Meeker [15], the total degradation is a function of time and dosage. Therefore, a model has been presented to determine the total effective dosage required for complete degradation. However, the model presented does not provide an estimate for the time taken by the material to degrade at the incident intensity of light. This model also requires to have the spectral irradiance of the light source as a function of the wavelength along with other material related parameters like the spectral absorbance of the material along with the quasi quantum absorption efficiency.

The total effective UV dosage at real time t can be expressed as

$$\mathrm{D}_{\mathrm{Tot}}(t) = \int_0^t \mathrm{D}_{\mathrm{Inst}}(\tau)\, d\tau$$

$$\begin{aligned}\mathrm{D}_{\mathrm{Inst}}(\tau) &= \int_{\lambda_1}^{\lambda_2} \mathrm{D}_{\mathrm{Inst}}(\tau, \lambda)\, d\lambda \\ &= \int_{\lambda_1}^{\lambda_2} E_0(\lambda, \tau) \\ &\qquad \times \{1 - \exp[-A(\lambda)]\}\phi(\lambda)\, d\lambda.\end{aligned}$$

Where E0 (λ, τ) is the spectral irradiance of the light source at time τ as a function of the wavelength [1 – exp (−A (λ))] is the spectral absorbance of the material being exposed (damage is caused only by photons that are absorbed into the material), and φ(λ) is a quasi- quantum efficiency of the absorbed radiation and CF is an “acceleration factor.”

$$\begin{aligned}d(t) &= \mathrm{CF} \times \mathrm{D}_{\mathrm{Tot}}(t) \\ &= \mathrm{CF} \times \left[\int_0^t \int_{\lambda_1}^{\lambda_2} \mathrm{D}_{\mathrm{Inst}}(\tau, \lambda)\, d\lambda\, d\tau\right]\end{aligned}$$

### 2.5.1 Reciprocity law

According to Avenel et al. [40], the fundamental law governing photo-degradation of polymeric materials is the reciprocity law which states that degradation is a function of intensity and time together and is independent of each one of these elements independently. That is, the product of intensity with time taken for complete degradation is a constant. However, experimental results in many cases show deviation from the law. Bunsen and Roscoe [41] were the first to conduct reciprocity law experiments to analyze the change in photo-response of a substance versus the radiant flux. Their research concluded that mechanisms governing the photochemical reactions solely rely on the cumulative energy absorbed by the material. The absorbed energy is given by two factors which are the Radiant flux/intensity (I) and the exposed time (t). This conclusion was later regarded as the reciprocity law and given as follows;

$$It = \text{constant} \qquad \text{(eq. 1)}$$

As the reciprocity law is only dependent on the cumulative absorbed energy by the material, its validation experimentally can have different forms of experimental methodology. Integrated area under each one of the four experimental forms represents the absorbed energy. This means that as the absorbed energy for these different forms would be the same meaning the material would degrade in an equivalent manner regardless of the experimental form granted the reciprocity law is conformed. Figure 8 below represents four different experimental approaches to exposing a material to incident flux:

a) High incident flux for a short exposure time

b) Low incident flux for a long exposure time

c) High incident flux with on/off cycling at high frequency

d) Varying the incident flux level during the exposure time and keeping it constant for a specific time.

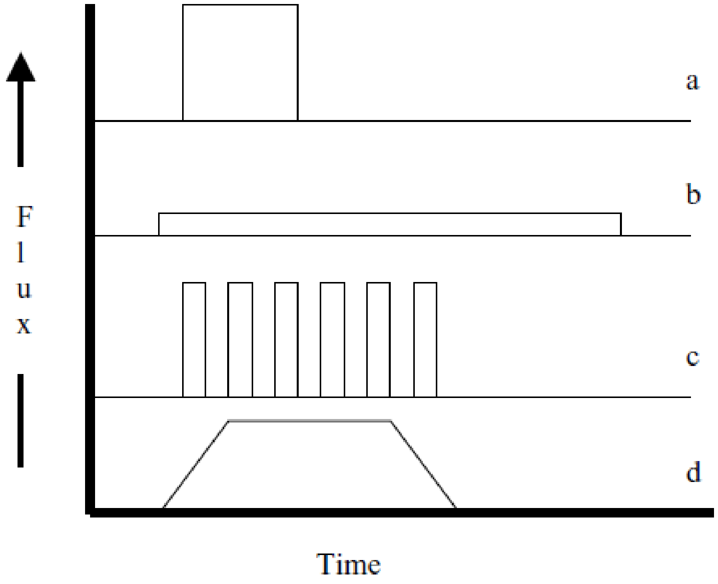

**Figure 8: Different experimental approaches to expose the sample to concentrated flux, reprinted from [37]**

Schwarzschild modified the equation (eq 1), introducing a factor, p, Schwarzschild's constant which accounts for the deviation from the theory. Schwarzschild found p = 0.86 but future research shows that p varies from material to material. Martin et al. [37] summarized the findings of Schwarzschild as the Schwarzschild's law and reciprocity law are widely used for determining the photoresponse of the material with respect to the incident intensity. According to Schwarzschild's law,

$$I^p t = constant \qquad \text{(eq. 2)}$$

or

$$It^p = constant \qquad \text{(eq. 3)}$$

Where I is the intensity of light provided to the sample and t is the time taken for total degradation. Equation 2 and 3, using the experimental data obtained for total degradation at different intensities, are used to determine the value of p and constant. The value of p depends on the material. It differs for different materials and even shows variation when the incident flux values change. The value of p = 1 shows that the material follows the reciprocity law. Therefore, the values of p are determined for P3HT-PCBM mixture as well as P3HS-PCBM mixture after confirming if the data follows Schwarzschild's law. The values for Schwarzschild's constant and known constants (equation 1 or 2) are used to generalize and predict the lifetime of the material at the incident flux provided.

### 2.5.2 ASTM models on accelerated weathering techniques

The American Society for Testing and Materials (ASTM) also provides a fundamental guide to statistical methods used to interpret weathering tests (G169) [42]. The methods presented in the standard are both applicable to the outdoor and laboratory weathering tests. Figure 9 provides a basic flowchart/algorithm for selecting the post processing method to be used to analyze weathering data. In our case as the response variable, absorbance of the material, is quantitative and the number of predictor variables is one and it's continuous, we can use the regression method; which again aligns with the method proposed by meeker [15] and the reciprocity law [37].

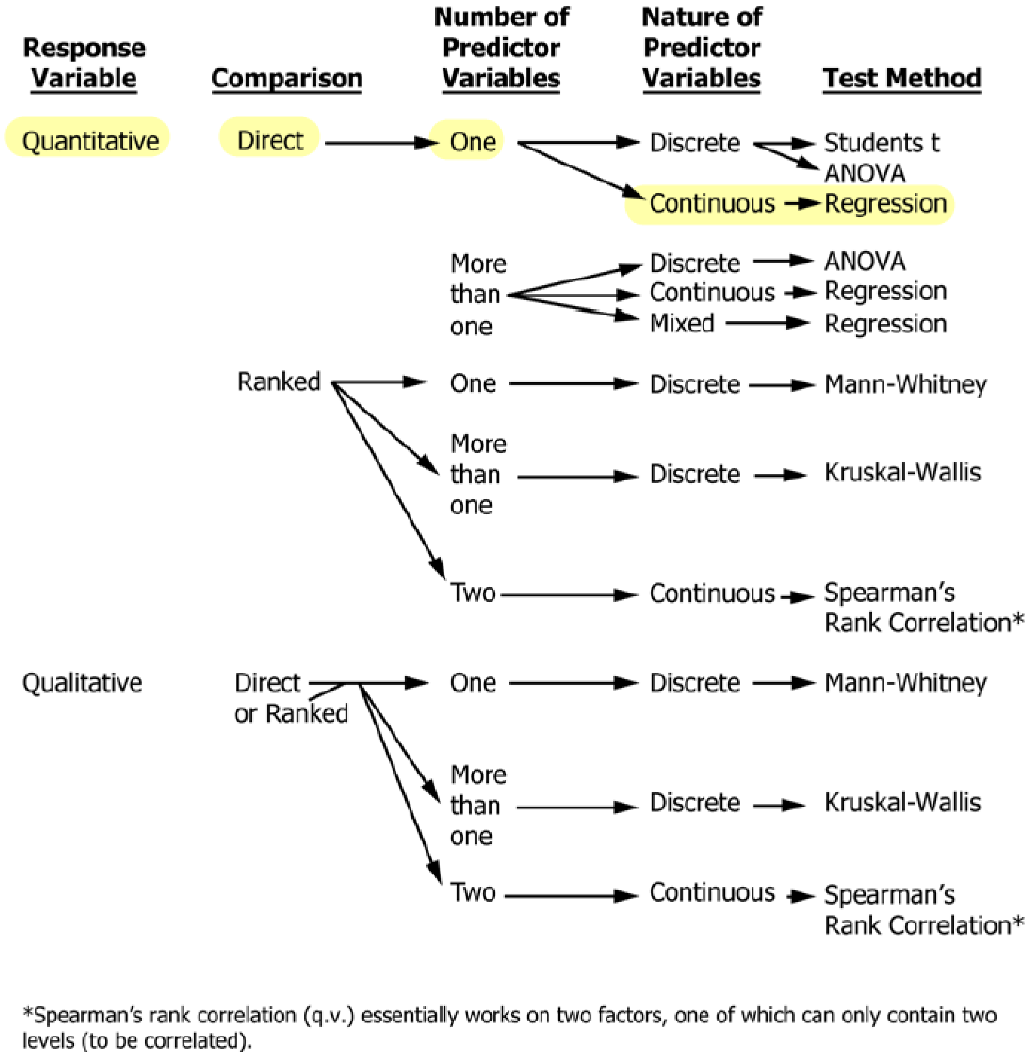

**Figure 9: Flowchart for selecting a method for post-processing data, reprinted from [42]**

The standard suggests basic linear regression the case of one variable change; in which each predictor variable is plotted against the corresponding measurement as a discrete value on the x-y plane. Regression can also be adapted to more than one predictor factor and also accommodate non-linear models. The standard provides a similar hypothesis to the Schwarzschild law where when two data points are plotted at different exposure values and when a third point is plotted, it lies on the line, this means that the experimental data is in agreement with each other, also known as a correlation. The standard suggests that for accurate interpretation of the weathering data, the data points should be well spaced because uneven spacing might give oddly high R2 values [42].

ASTM standard G-141 talks about the variability in the results of exposure testing using nonmetallic materials. The standard advocates poor reproducibility of test results because of multiple aspects; mainly including the material type and homogeneity, the complexity in terms of outdoor testing and precisely controlling the laboratory experimental parameters. The standard also discusses the variability in the post treatment after exposure and being precise with tests conducted in one lab compared to the other [43]. This research provided an alternative that directly tackles the concern discussed in the ASTM standard G141. The standard stresses on the fact that the repeatability of experimental results depend mainly on the material and the material property being measured.

ASTM standard G-172 Statistical Analysis of Accelerated Service Life Data provides statistical tools using the Arrhenius model with a given probability of failure and the Weibull model [44]. Both of these models require material specific constant parameters to be used and the models are not specific to accelerated photo-degradation studies. Hence the calculations presented later in the report are based on the photo-degradation model presented by Escobar and meeker and the reciprocity law.

# 3. RESEARCH METHODOLOGY

## 3.1 Experimental setup

### 3.1.1 Development of the facility

As it can be seen in figure 10, the Ultra-High Flux Solar Simulator (UHFSS) was lacking several key auxiliary equipment/modifications to be ready for commissioning. The first deliverable of the project was to complete these modifications in six month to be able to continue with the design and execution of experiments. A brief list of the modifications is given below along with the overview of the completed facility.

A. Custom structural design and modifications
B. Installation of a custom bench for the Gas Chromatography (GC) machine
C. Design, acquisition and installation of state-of-the-art Flow and pressure control modules
D. Installation of a custom fume hood for the reaction chamber and exhaust for the GC.
E. Installation of independent refrigeration unit along with the Air ducts and the roof.
F. Design and installation of a modular workbench for the target area
G. Installation of a 3-axis movement controller (accuracy of 0.1 mm)
H. Installation of piping and fittings for tap water and standalone cooling using a Julabo FT-1600 cooler.

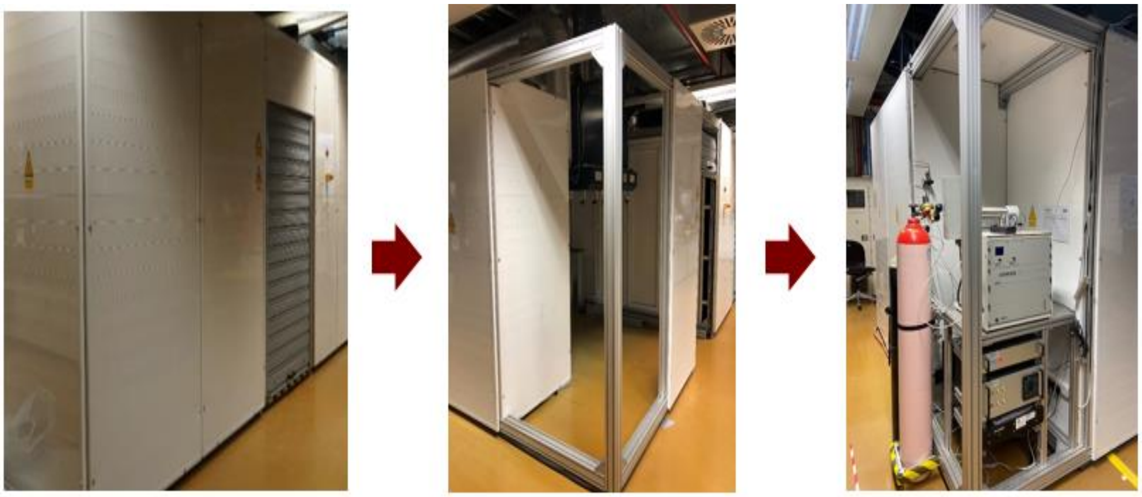

**Figure 10: Overhaul process of the outside of the UFHSS**

The UHFSS consists of seven 6kW Xenon short arc lamps by Osram as shown in Figure 11. The system is designed and capable to provide energy in excess of 3000 kW/m2 on 400 cm2 area. The incident flux can be concentrated on a 60mm diameter target at a focal distance of about 3m, attaining temperatures in the range of 2000°C. The Xenon lamps are favored as their emission spectrum resembles solar spectrum.

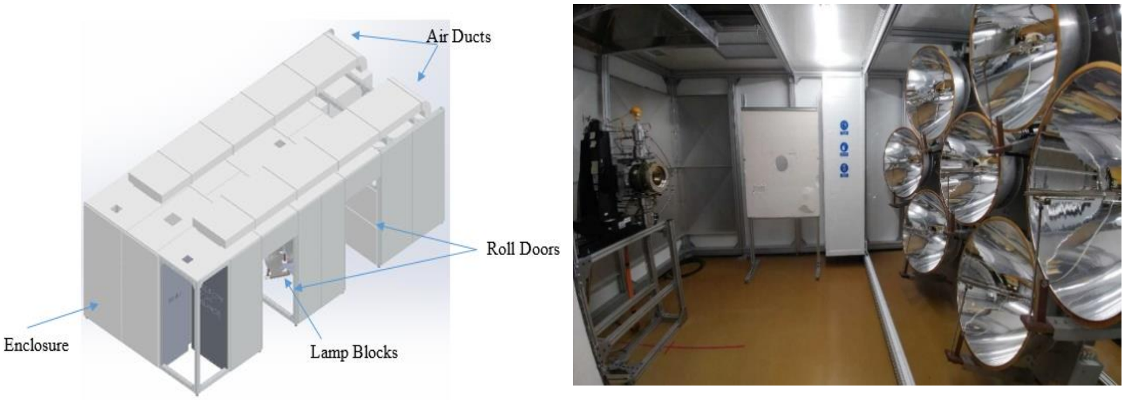

**Figure 11: (i) Isometric view of solar simulator and (ii) picture of the UHFSS interior**

A water-cooled lambertian target (250 x 250 mm) is mounted on a three axis movement controller in the focal plane of the seven lamps. The lambertian surface of the target ensures that the incident light is diffused/reflected equally in all directions. Hence, regardless of viewing angle, the target reflects light equally and appears with the same brightness .This allows the charged-coupled device (CCD) camera to be mounted at various angles to capture the images. The three axis movement controller has an accuracy of up to ± 0.1mm in the all three axis. The lambertian target has a hole in the middle (1 inch) where a water cooled heat flux gage is installed. The flux gage generates an output voltage signal which correlates to an incident flux value. The raw voltage received from the flux gage is processed using the manufacturer's calibration curve. The flux gage is calibrated t measure up to 5000 kW/m2. Both the Lambertian target and the flux gage are water cooled and the system and multiple contact type J thermocouples installed to ensure no overheating takes place. A schematic is illustrates the targets and positions of the thermocouples below. The image acquisition was done using an 8 bit (CCD) camera along with several neutral density (ND) filters to protect the image sensor from the extreme intensity of light. The experimental setup is shown in figure 12.

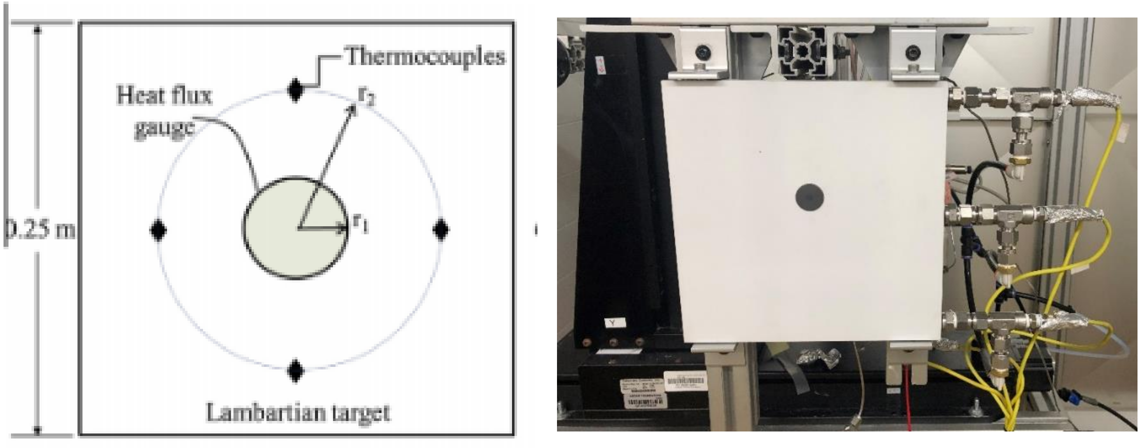

**Figure 12: Schematic illustration of lambertian target and the actual experimental setup**

### 3.2 Flux characterization

Flux mapping method was used to carry out the flux characterization of the UHFSS. This allows the user to measure the flux distribution of an incident flux without the need of any direct measurements with a heat flux gage. The experimental setup is defined in the previous section. The basic idea of flux mapping is to correlate the measure incident flux values to the grayscale values on the images collected by the CCD camera. The grayscale values of an image are the brightness values of the individual pixels of the image. The end result is to have each pixel of the image associated with a specific flux value.

Incident flux values across the entire lambertian target were recorded on the three axis with multiple images at different exposure values. A semi-automated LabVIEW program was designed and is able to measure and record incident flux values, images from the CCD and temperature values from the setup as programed. The flux values were calculated in the positive and negative, x and y axis in three segments. Segment A is comprised of 1 cm diameter from the center point and the flux values were recorded at 0.25 mm interval. Segment B is an annulus with the inner diameter of 1 cm and outer diameter of 3cm, and the flux values were recorded at 0.5 mm interval. Segment C is an annulus with the inner diameter of 3 cm and outer diameter of 5 cm, and the flux values were recorded at 2 mm interval. Additional measurements were also taken at 2 mm intervals to check spatial non-uniformity and verification of the characterization. This data collection methodology was adopted because the emission spectrum from the Xenon arc lamps follows a Gaussian distribution and hence the flux values drop significantly when the distance from the center increases. The flux values were recorded at a frequency of one measurement per second for 30 secs, at each position and then averaged for processing. This averaging minimizes the error percentage and also helps reduces the standard deviation. 40 images were also obtained at different exposure values (1/200s, 1/1000s, 1/1250s and 1/2000s) and then averaged for processing.

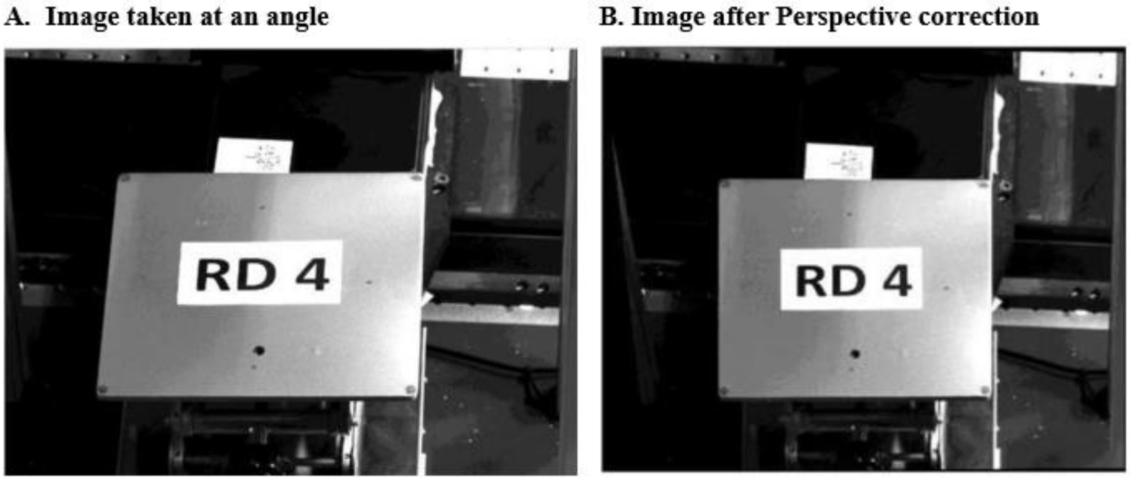

**Figure 13: An example of perspective correction algorithm used**

The images captured were processed using MATLAB with processing techniques like perspective correction and image averaging. An example of the perspective correction technique is shown in figure 13. The images were converted into a matrix based on the resolution of the 8 bit camera and then that matrix was average to reduce the background noise. Perspective correction is done using a projective transformation algorithm to reduce the distortion in images because the images were taken at an angle. This reorientation would allow the images to have the exact dimensions of the target and hence the pixel values and the flux values can be accurately correlated. The processed images are depicted below in figure 14;

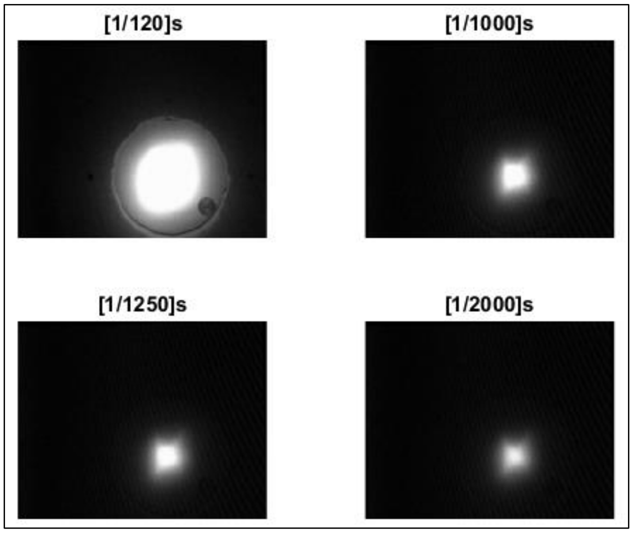

**Figure 14: Flux images at different exposures**

These images are then processed by taking a weighted average of the combined exposure and getting one normalized image using the equation 1 below. This results in a single image containing data from all exposures, which is depicted in Figure 15.

$$\text{Normalized image}(i,j) = \sum_{n=1}^{N} \frac{P_n(i,j)}{t_{expo,n}} \qquad \text{(eq. 4)}$$

Where $P_n(i, j)$ is the greyscale value of the pixel (i,j) in the image with exposure n and $t_{expo}$ is the exposure time.

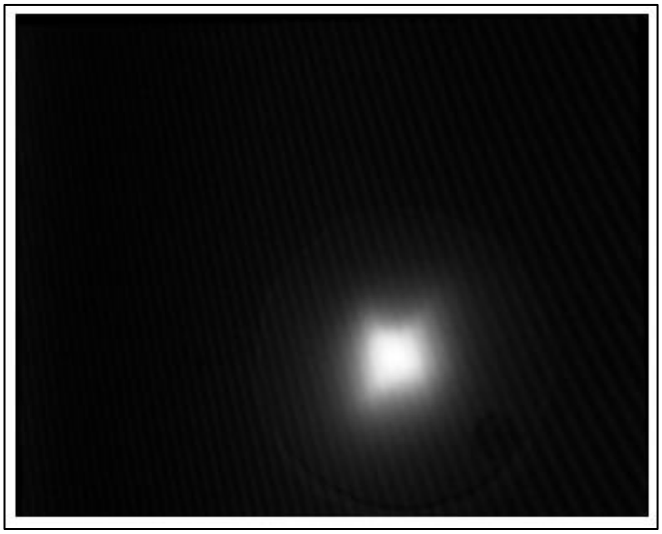

Figure 15: Weighted flux average taken from four different exposures

The heat flux gage has a diameter of 2.53 cm (approx. 1 inch). Hence, the greyscale values of a similar arbitrary area were averaged to be used and correlated to the measured flux values. This arbitrary area was moved in a similar pattern that was used to calculate the flux values earlier using the 3 segments. The characterization curve was obtained by plotting the incident flux values against the greyscale values. The characterization curve for positive and negative X axis is given in figure 16 and the characterization curve for the positive and negative Y axis is given in figure 17. A linear curve fitting was done and the $R^2$ value of 0.989 was obtained. This calibration curve was used in the MATLAB code to generate flux distribution map on the lambertian target. Flux mapping with the help of the calibration curve obtained can provide the flux distribution on any surface with limited measurements. The flux map can be used to analyze images of the setup and the incident flux values can be estimated without the use of a flux gage to measure. The overall calibration curve is given in figure 18 below;

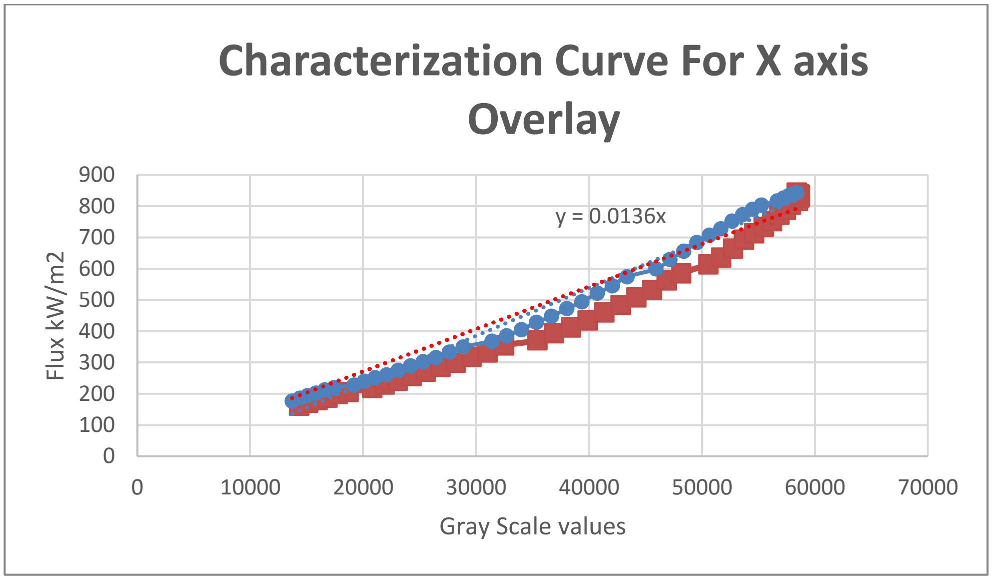

**Figure 16: Characterization curve obtained from the positive and negative x-axis**

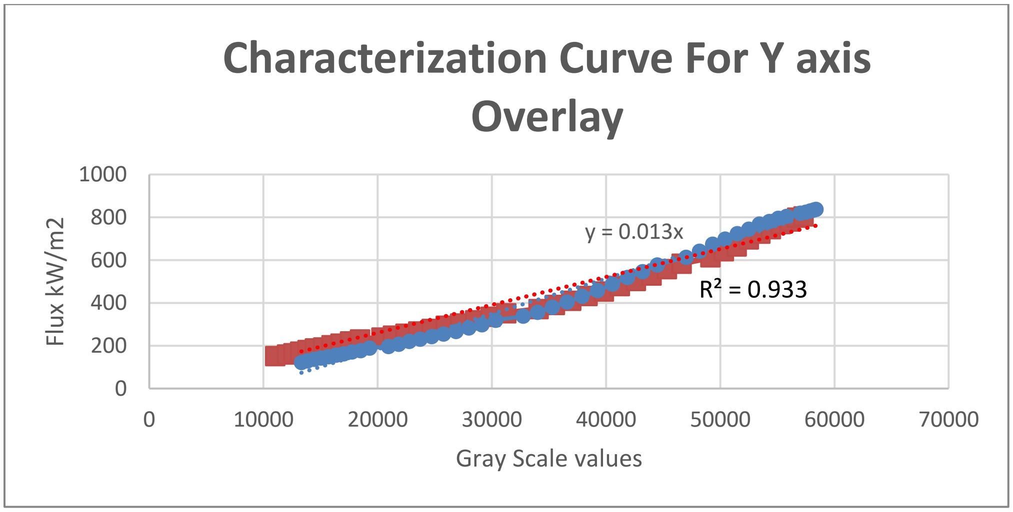

**Figure 17: Characterization curve obtained from the positive and negative y-axis**

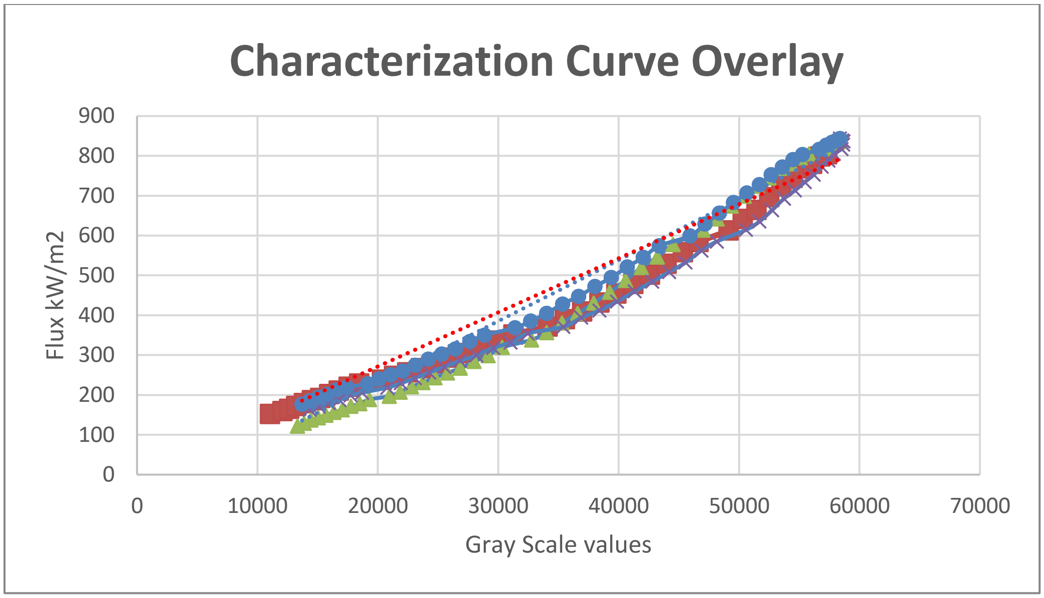

**Figure 18: Characterization curve overlay for a single lamp characterization**

The characterization curve obtained is linearly fitted with an $R^2$ value of 0.989. The equation of the line from the curve is used in the MATLAB code to produce the flux distribution maps. Using the MATLAB code, the grayscale value of an individual pixel in the image is substituted with the corresponding value of the incident flux based on the calibration curve. Figure 19 shows the flux distribution map generated based on the characterization curve that was calculated earlier to convert the average greyscale image in Figure 18. The flux distribution map illustrates concentric circle profiles which is as expected. Therefore, the proposed system to characterize the incident flux and generate flux distribution map is functional. The gaussian overlay of the flux distribution along the X and Y axis is given below in figure 20. The contour plot obtained after the matlab processing is given in figure 21.

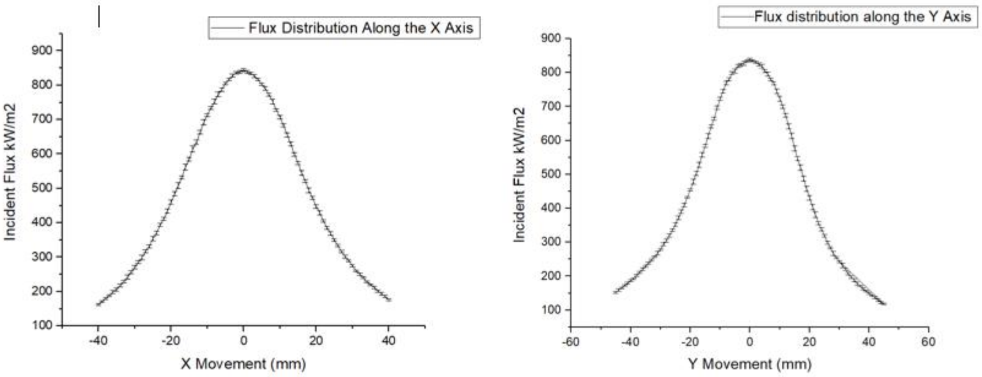

**Figure 19: Gaussian flux distribution along the x and y axis for a single lamp**

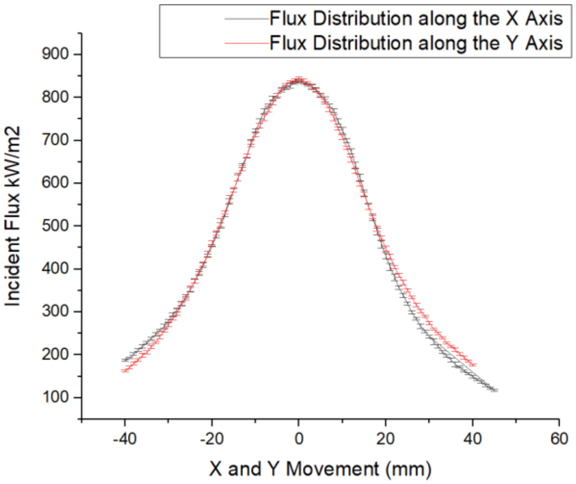

**Figure 20: Gaussian flux distribution overlay for a single lamp**

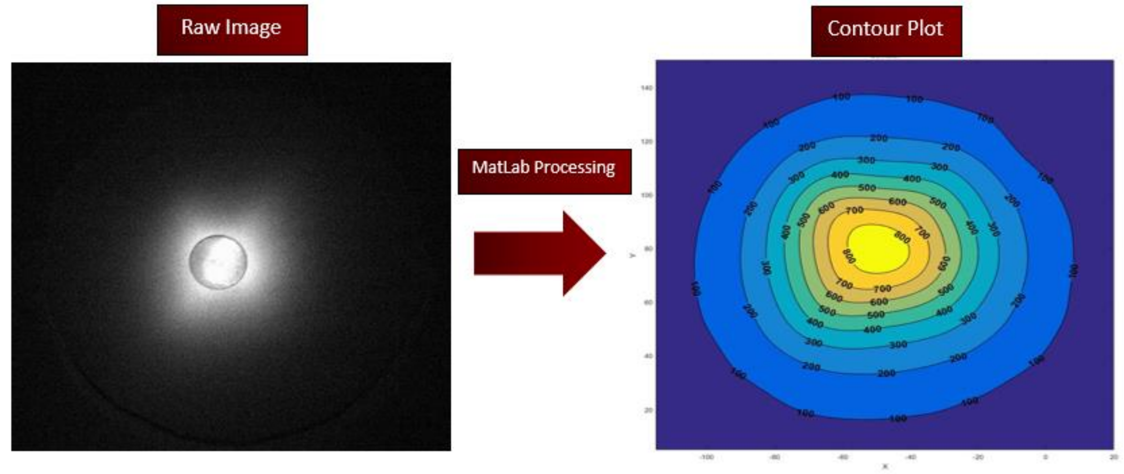

Figure 21: Contour plot obtained for the characterization of a single lamp

## 3.3 Experimental aging setup

### 3.3.1 Open setup

As the output flux of the UHFSS has a Gaussian distribution, a light collimator is used to homogenized the incident flux that sample receives. The light collimator is a hexagonal fused silica light pipe by Edmund optics having an exit and entrance aperture of 10 mm and a length of 125mm. The collimator as excellent UV transmission and is rated for a wavelength range of 200-2200 nm. The light collimator is located at the focal point of the UHFSS and is perfectly aligned with the optical axis using optical accessories by Edmund optics. The light pipe is held in place by custom made ceramic holders that prevent the light pipe from thermal shock and still allow position to be adjusted accurately. A heat flux gage is placed right after the light collimator to measure the intensity of the incident flux at that particular distance. The heat flux gage is a water cooled Gardon-type circular foil radiometer by Vatell and the model number is TG1000-0. The flux gage has a min and max range of 5 W/cm2 and 5000 W/cm2 respectively. The sensor has a repeatability of 1% and an accuracy of ± 3%. The sensor contains a colloidal graphite coating on the front face giving it a sensitivity of up to 2mV/(W/cm2) Hence the front of the sensor is not supposed to be touched or tampered with. An aluminum cylindrical heat exchanger resembling the heat flux gage was fabricated to cool down the samples while being exposed to the ultra-high flux levels. The heat flux gage is used to setup the experiment and then it is replaced by the aluminum heat exchanger to carry out the experiment once the flux intensity is characterized. Both the Heat exchanger and the flux gage are cooled by using a Julabo FC1600T recirculating cooler having a temperature stability of ±0.2 $^{o}$C and it uses distilled water as the cooling medium. The entire assembly is mounted on a perforated bench that fits the optical accessories. The bench is attach to a three-axis movement controller by Newmark which allows the precision positioning of the setup in the focal plane. The slides for the x, y z axes of the controller are NLS8-500-101, NLS8-300-102, and NLS8-200-101 respectively. The controller has a 1 μm repeatability rating with precision slides with a resolution of 0.08 μm. The sample, which in this case is a polymer coated on a glass substrate is mounted on the front face of the heat exchanger using a thin layer of ceramic thermal paste. The paste allows a better heat transfer between the sample and the exchanger along with helping to mount the sample on the exchanger without the need for an external holder. The entire setup has multiple contact type-J thermocouples on multiple surface along with a type K infrared IR temperature sensor that is used to measure the temperature of the polymer coated on the glass substrate. The data acquisition is done using I/O modules NI-9211 and NI-9213 by National instruments and the modules are installed in a CompactDAQ chassis cDAQ-

9178. The Chassis is connected to a PC using an Ethernet cable and the data is processed using LabVIEW 17.0.

### 3.3.1.1 Pros/Cons of the open setup

The heat exchanger the sample is mounted to, gives independent temperature control of the sample by maintaining the temperature independently of the incident flux. This allows us to conduct experiments that study independently the photo-degradation of materials or a combination of thermal and photo-degradation of the material. Being an open setup the system is independent of the sample size and allows the users to be flexible in the setup. The setup is shown in figure 22.

The downside of using an open setup is the lack of parameters that can be controlled during experimental design. This open setup lacks the capability of carrying out experiments where the environment the sample is exposed to is controlled for example, inert atmosphere, vacuum conditions, relative humidity and salinity are a few factors that cannot be controlled in this setup.

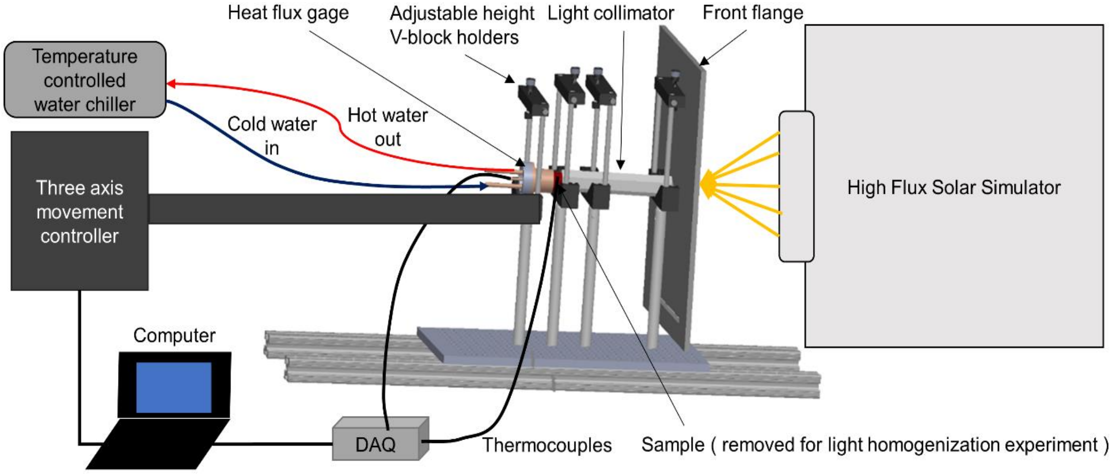

**Figure 22: The proposed preliminary solar aging setup; schematic and actual (past experience)**

### 3.3.2 Reactor design

In order to test different materials using the UHFSS, a solar cell was necessary that can be used to test the samples in different experimental conditions. The current setup, with the open design limits the experiment to be run in a batch mode. This limits the user to have to manually take out the sample at known intervals, prepare it for UV-VIS characterization and then re-run the experiment to calculate the reduction in absorption performance of the sample. This process is tedious and also has the potential of having a degree of human error attached if the sample is mishandled in between the process. The main idea of the reactor design is to be able to continuously measure and record the absorption spectrum of the sample as it is being exposed to the incident flux to generate a seamless degradation plot over time. During the literature review, a solar cell design was found with supposedly similar online optical characterization potential presented by Hintz et al [45] . The design presented lacked the ability to control certain key experimental parameters like, temperature control, exposure to different atmosphere, humidity etc. The apparatus presented in this thesis aims to overcome all of those challenges. The concept presented by Hintz et al. is depicted in figure 23 below;

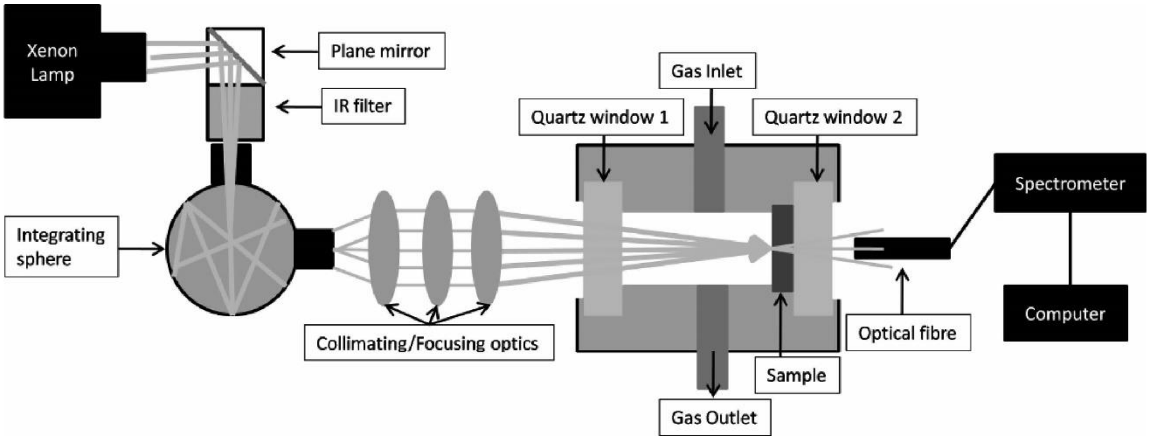

**Figure 23: Photo-reactor design proposed, reprinted from [45].**

The reactor would need to be a sealed chamber so the polymer can be exposed to a controlled environment. It also needs to acts as a heat exchanger to control the temperature of the sample. Multiple designs were considered and the a final reactor design which was proposed is given in the figure 24 and figure 25 below;

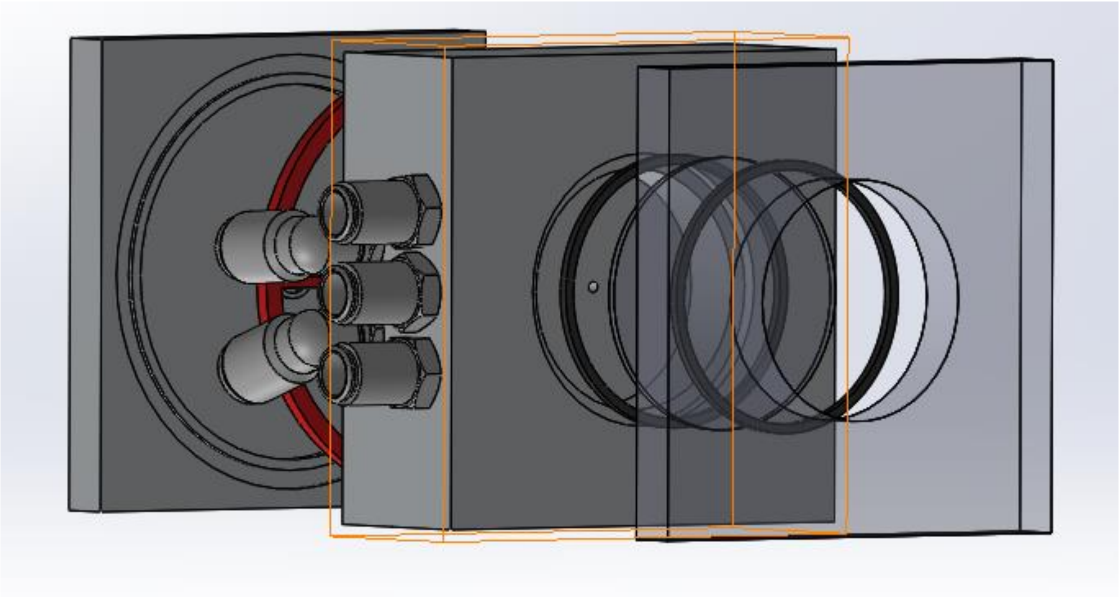

**Figure 24: Front view of the designed photo-reactor**

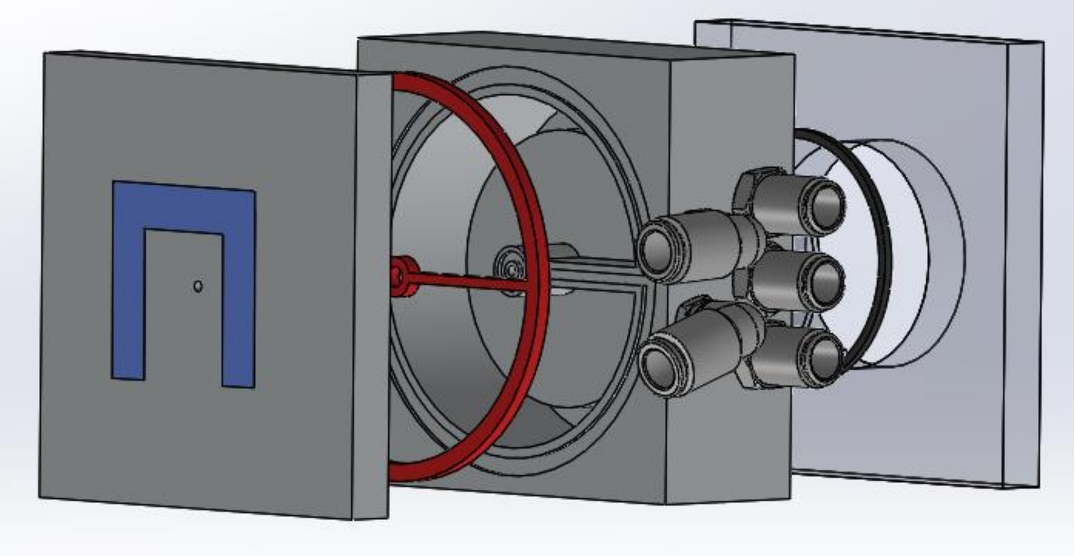

**Figure 25: Back view of the designed photo-reactor**

### 3.3.3 Closed experimental design

The closed experimental setup to conduct continuous degradation experiments is given in figure 26 below. The light enters from the left passing through a small hole in the ceramic shield and going through the light collimator to onto the sample. The sample temperature measurement is taken using an IR thermometer. The cell has a multiple probe and contact thermocouples to monitor the temperature during the experiments. The back side of the cell houses a cooling jacket that cools the sample as well as keeps the cell temperature from exceeding a safe limit. The sample cavity also contains gas inlet and outlet to control the ambient atmosphere to the sample. The light passes through the sample and is transferred using an optical fiber cable to the spectrometer to conduct the

UV-Vis analysis. The cell also houses a ND filter cartridge to reduce the intensity of light coming from the solar simulator to avoid any damage to the spectrometer.

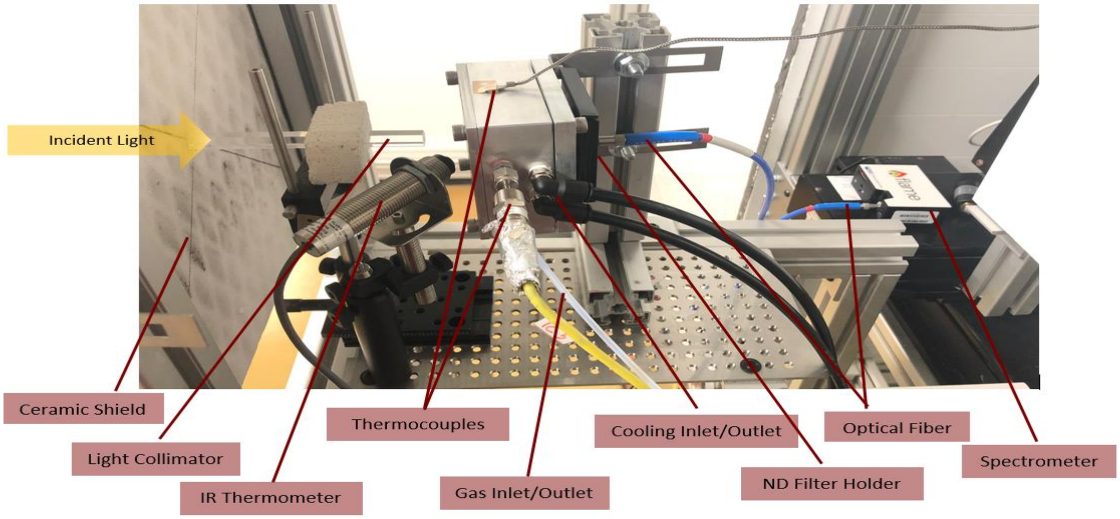

**Figure 26: Experimental setup for the continuous degradation experiments**

The newly designed apparatus was tested under experimental conditions with an intensity of 200 suns. The temperature of the apparatus was measured in three locations; A) Sample Temperature, B) Cavity Temperature and C) Cell Backside Temperature. The sample temperature was measured using an infrared thermometer aimed at the sample (± $6^{o}$C accuracy). The backside temperature was measured using a contact thermocouple and the cavity temperature was measured using a thermocouple probe suspended within the cavity. The cooling fluid was distilled water set at 25 degrees using a standalone cooler and the cooler has automatic variable flowrate to maintain the desired set-point. The sample temperature was successfully maintained at a desired set point of 40oC and the temperature vs time plot is given in figure 27. The pros and cons of the newly designed apparatus are given in table 3.

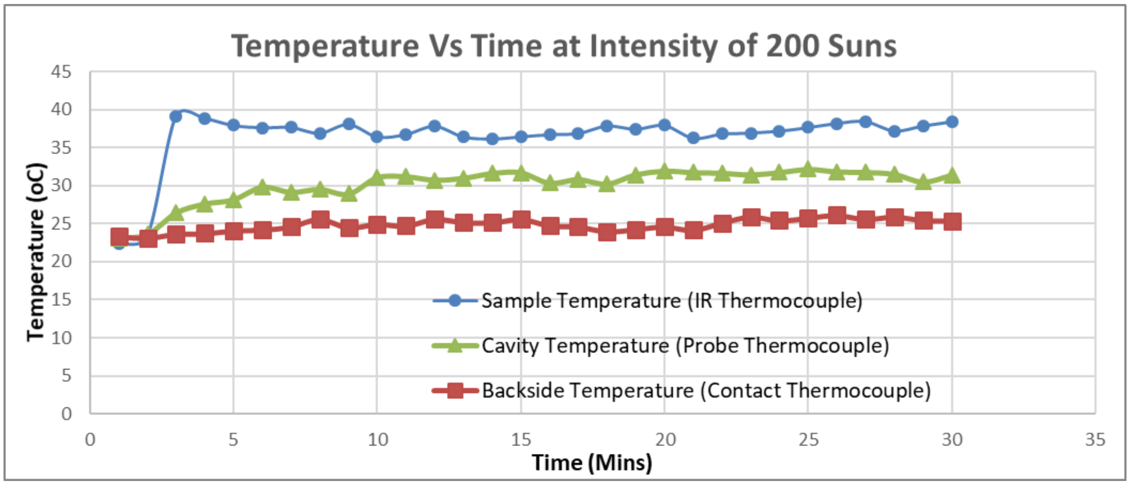

**Figure 27: Temperature vs time plot for the cell in operational conditions of 200 suns intensity**

**Table 3: Pros and cons of the designed apparatus**

| Pros | Cons |
|---|---|
| • Online optical characterization<br>• Accurate incident flux and temperature control<br>• Ambient atmosphere and humidity control<br>• Gases emitted by the reaction can be analyzed<br>• Modular design | • Limited by the sample size<br>• Requires optical alignment accessories to carefully place the sample surface at a similar position to the flux gage measurement (Human error possible) |

Novelty of the apparatus compared to the alternative testing methods:

1) Requires only a few milligrams of the sample to carry out the full testing and therefore can test the material during the early stages of life.
2) Testing duration reduced to just a couple of hours as a result of very high accelerated aging. Also, various exposure cycles can be programmed to emulate thermal shock and abrupt conditions.
3) The sample temperature can be controlled independently from the light source and ranges from ambient to more than 1,500$^{o}$ C . The light degradation mechanisms can be isolated and studied separately from the thermal ones.
4) Online collection of the light transmitted through the sample provides in-situ information of the sample’s optical properties and composition further reducing the amount of sample needed for testing.
5) Environmental conditions i.e. temperature, humidity, and atmosphere composition can also be controlled from inert to reacting while the evolved gases can be analyzed if necessary.
6) Thick and highly concentrated films can be analyzed using this technique because the incident flux is a lot greater in energy compared to the analytical

## 4. RESULT AND DISCUSSION

### 4.1 Sample preparation

The common thin film preparation techniques include; A) Spin coating B) Dip Coating C) Knife Coating D. Drop Casting; [46-49] which are illustrated in figure 28 below. The P3HT and P3HT- PCBM thin films used in this research were prepared using drop casting technique using a blended solution followed by annealing for an hour. Microscope glass slides (Fused Silica) were cut to a 2 x 4 $cm^2$ size and cleaned with iso-propyl alcohol, the slides were dried under compressed air. 10 mg of P3HT and 10 mg of PCBM (c-61) were dissolved in 1 ml of dry chloroform. The solution was stirred for one hour at 45 $^oC$ and then drop casted on a cleaned glass slide. The resulting film thickness was $3 \pm 2\,\mu m$. The samples were allowed to rest for an hour before carrying out any characterization techniques. The drop casting was carried out by making a square template on the cleaned glass surface using stripes of scotch tape 10 mm thick [48]. The solution was dropped on the template and then swiped across the 1 x 1 $cm^2$ sample area to make sure that the solution would spread evenly. The use of Chloroform as the solvent aided in a quick evaporation. After the annealing, the tape was carefully removed and the samples could be test or characterized after that.

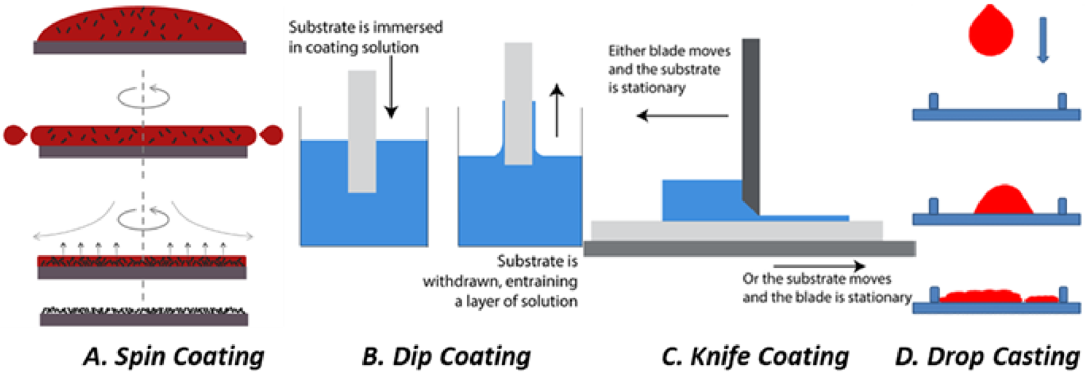

**Figure 28: Common techniques to prepare thin film samples**

The sample preparation technique was characterized and monitored using scanning electron microscopy and atomic force microscopy. The main criteria was the film thickness and the uniformity of the surface of the samples [50]. Two types of samples were characterized using SEM, The first sample had a single layer of the solution drop casted onto the glass slide and the second had two layers of the sample drop casted on to the glass slides. The SEM results are shown in figure 30 and figure 31. The resulting film thickness was confirmed to be 3 ±2 µm for the single layer and 6±2 µm for the dual layer drop casted sample. The results obtained of the samples prepared using drop casting are given in figure 29 below.

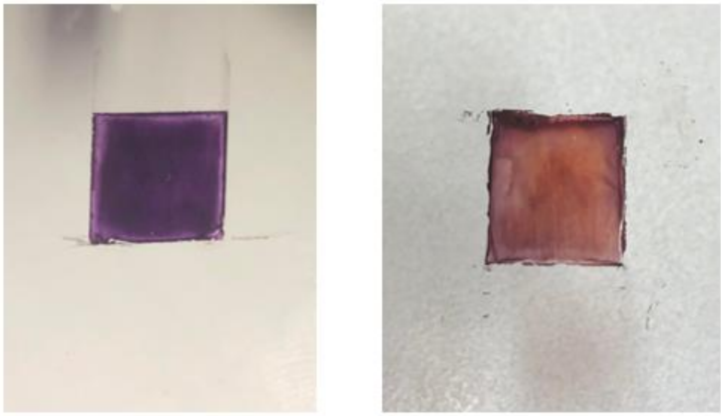

A) P3HT Film
B) P3HT/PCBM Film

**Figure 29: Prepared thin film samples**

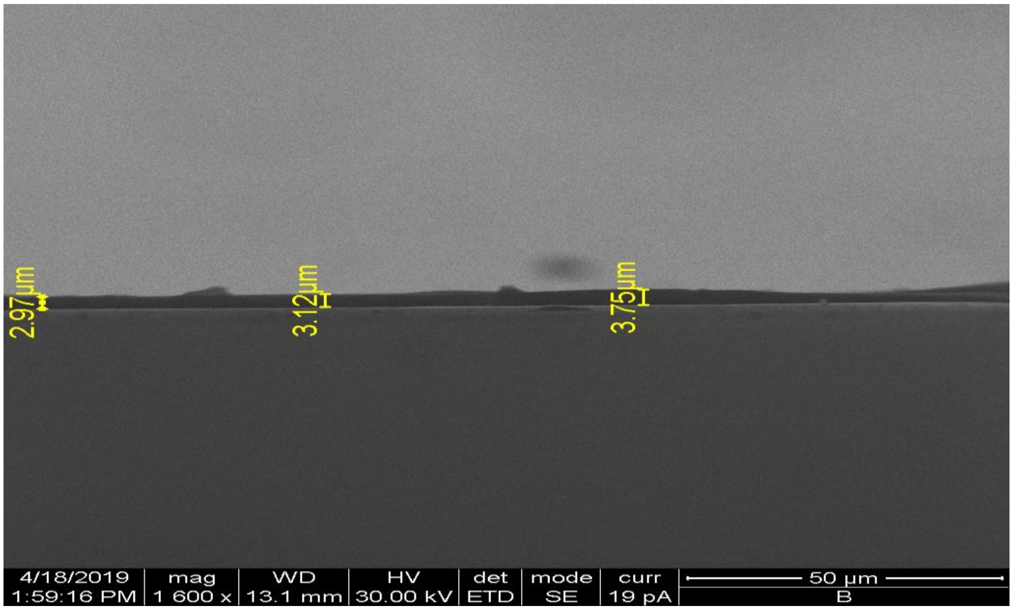

**Figure 30: SEM cross-section thickness of a single layer drop casted P3HT-PCBM film**

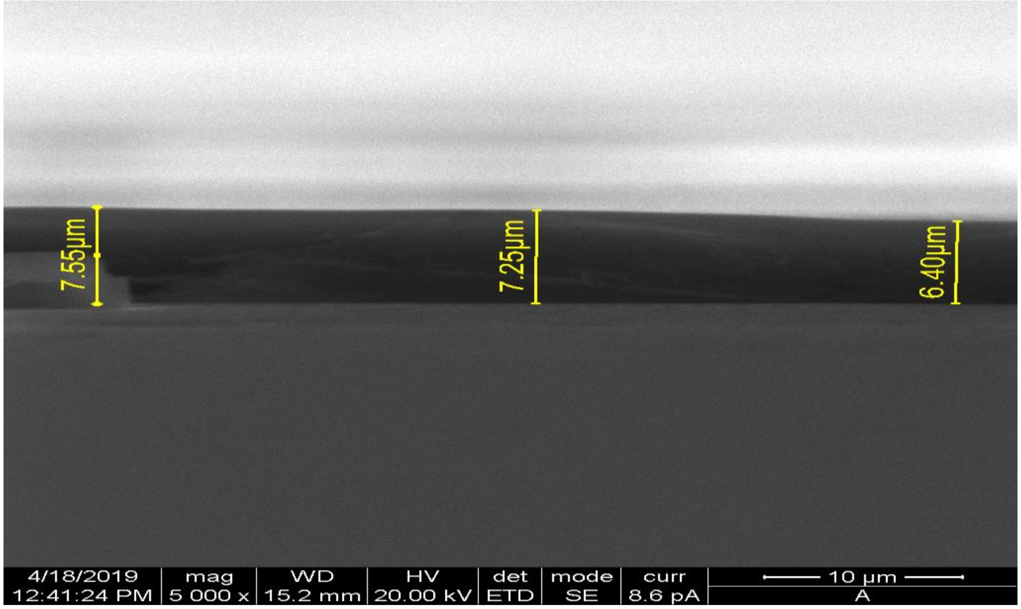

**Figure 31: SEM cross-section thickness of a dual layer drop casted P3HT-PCBM film**

The AFM results showed surface uniformity with a maximum and a minimum peak of 18.2 nm and -1.5 nm respectively. The resulting plot is given in figure 32 below.

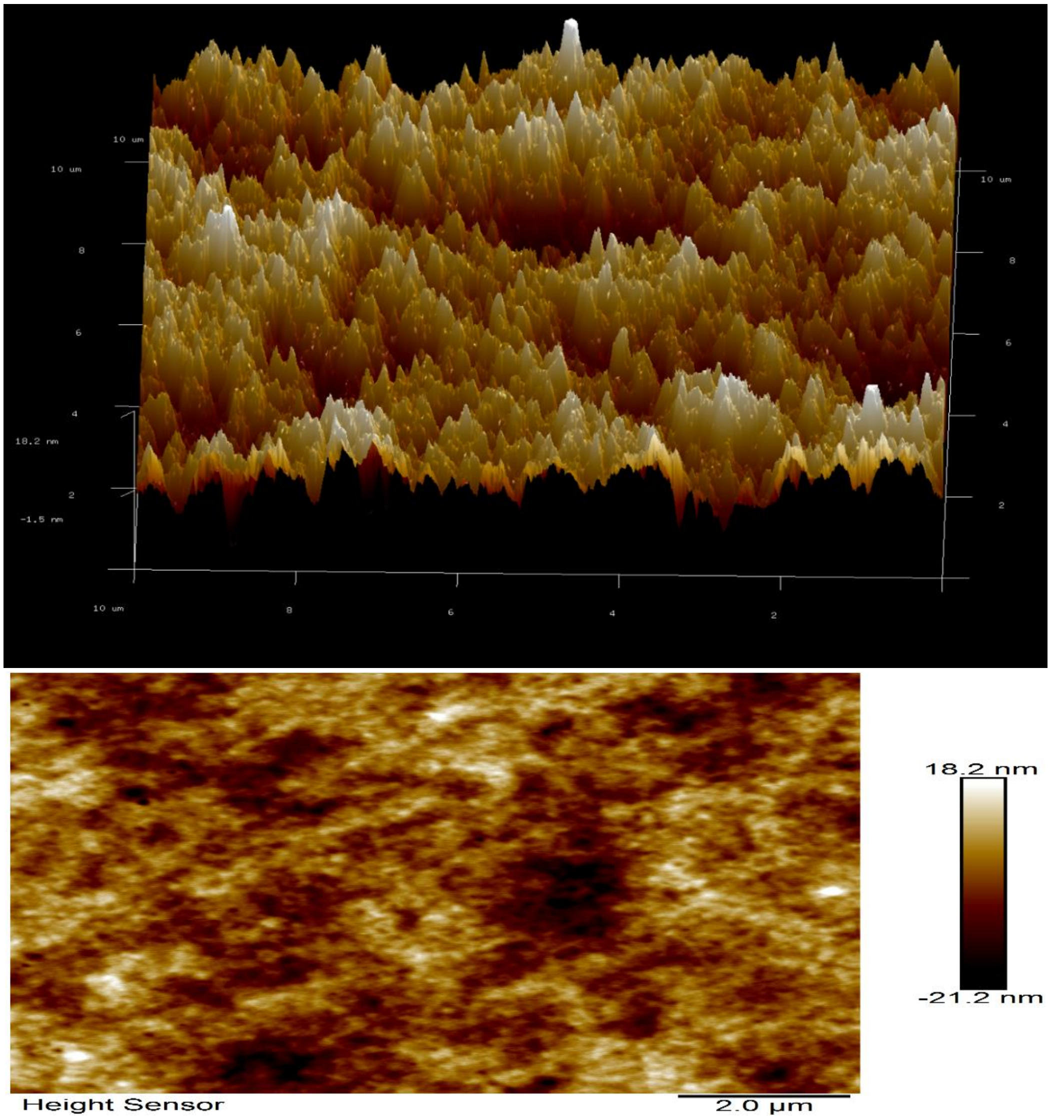

**Figure 32: AFM plot for single layer drop casted P3HT-PCBM film**

To further confirm the surface morphology of the prepared samples; SEM analysis was conducted to investigate the uniformity. The sample showed uniform coating throughout the sample with the feature size being in the nanometer scale. The detailed features in the nanometer scale were not visible clearly due to the limitation of the SEM Analysis equipment at the central materials lab at Texas A&M University at Qatar, which is rated for micrometer scale. The two images collected to analyze the surface uniformity are given below in figure 33 with the magnification of 500 and in figure 34 with the magnification of 50,000 respectively.

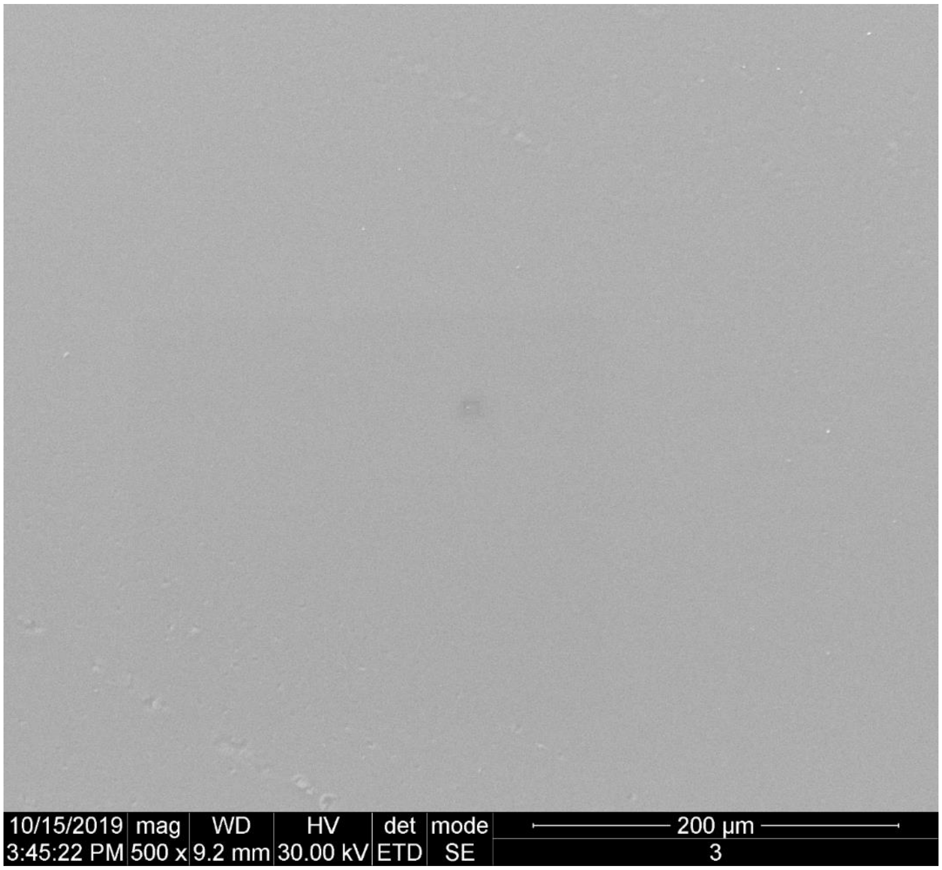

**Figure 33: Surface morphology of P3HT-PCBM film using chloroform solvent at 500x magnification**

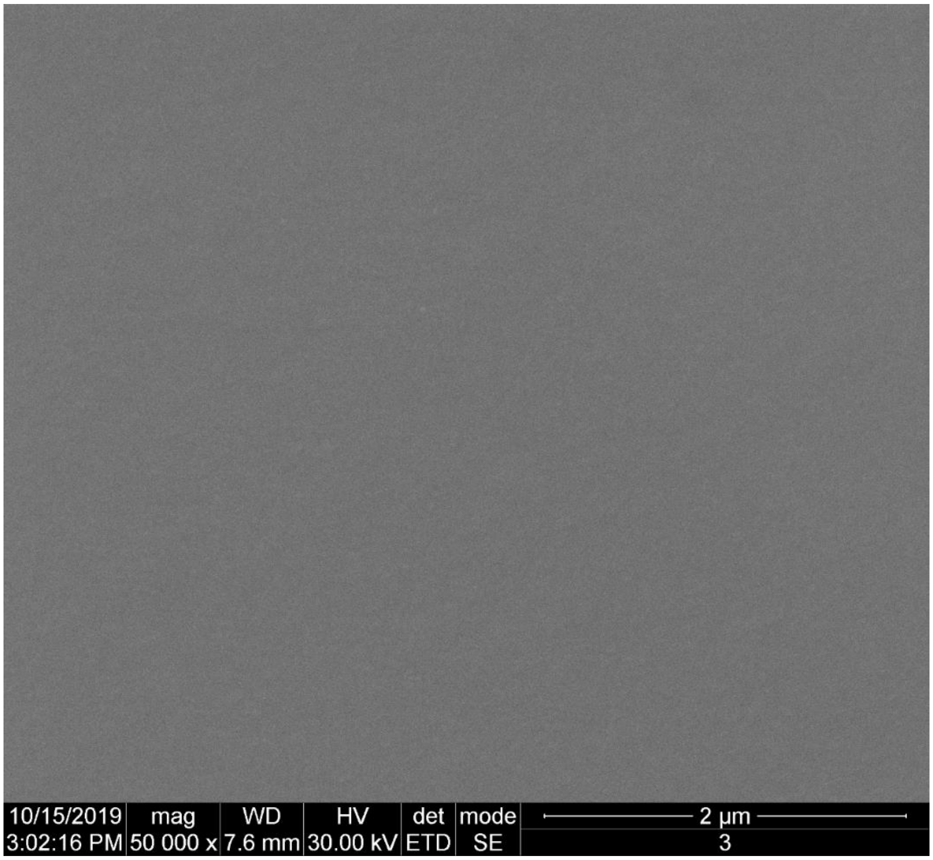

**Figure 34: Surface morphology of P3HT-PCBM film using chloroform solvent at 50,000x magnification**

## 4.2 UV-VIS analysis

UV-Vis spectrophotometry is a quantitative analysis to measure and study the light absorbance of a chemical substance. This is done by exposing the sample to a UV and visible light source. The light is separated into individual wavelengths and the incident beam is split into two beams; one of which passes through the reference and the other through the sample. The differential absorption is measure by a receiver and results generated [51]. The conventional UV-Vis Technique is time consuming and for this comparison a PerkinElmer LAMBDA 950 UV/Vis Spectrophotometer was used from the chemistry instrumentation lab. This spectrometer was compared to a miniature ocean insight spectrometer capable of measurement with response time of milliseconds. On the other hand, the conventional technique take 1-2 minutes per scan and it is impossible to have that unit connected to the photo cell to have continuous optical characterization.

In the comparison below illustrated in figure 35, the overall peaks of the spectrum align perfectly however the miniature spectrometer does lack the resolution to identify the shoulders at 560nm and 610nm granted the miniature spectrometer reads the data every one sec compared to 1-2 mins. This current data was averaged. This may be something that can be looked into during future work where multiple scans can be averaged to increase the resolution of the absorption spectrum.

The UV-VIS Absorption spectrum was carried out before and after the exposure, the absorption units were normalized to 1 and the absolute differential values were calculated. Average differential values were calculated for the wavelength range of 350-700 nm and these values were taken to be degradation percentage.

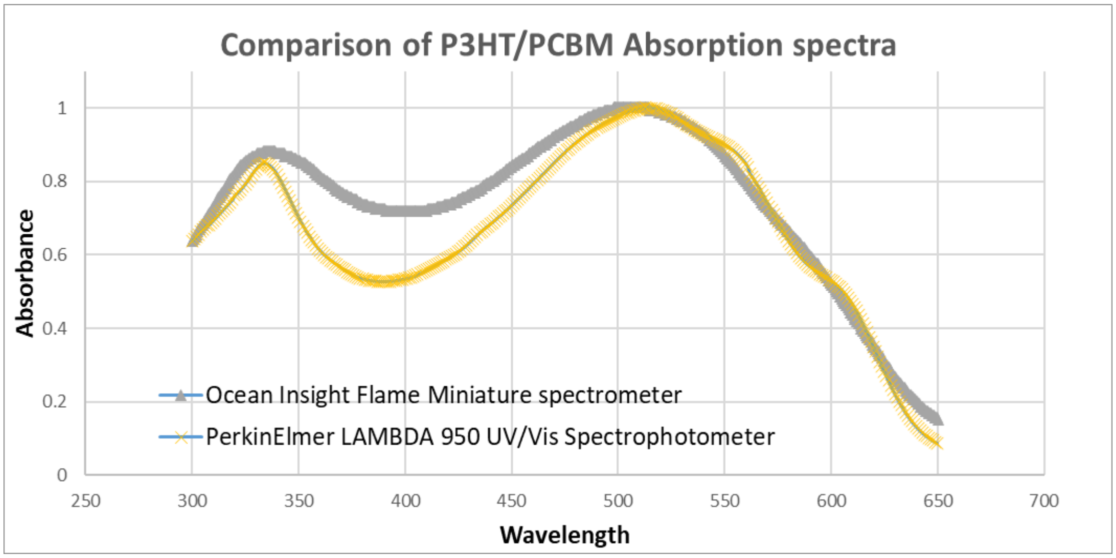

**Figure 35: Comparison of conventional UV-VIS Spectrometer to a miniature spectrometer**

### 4.2.1 P3HT

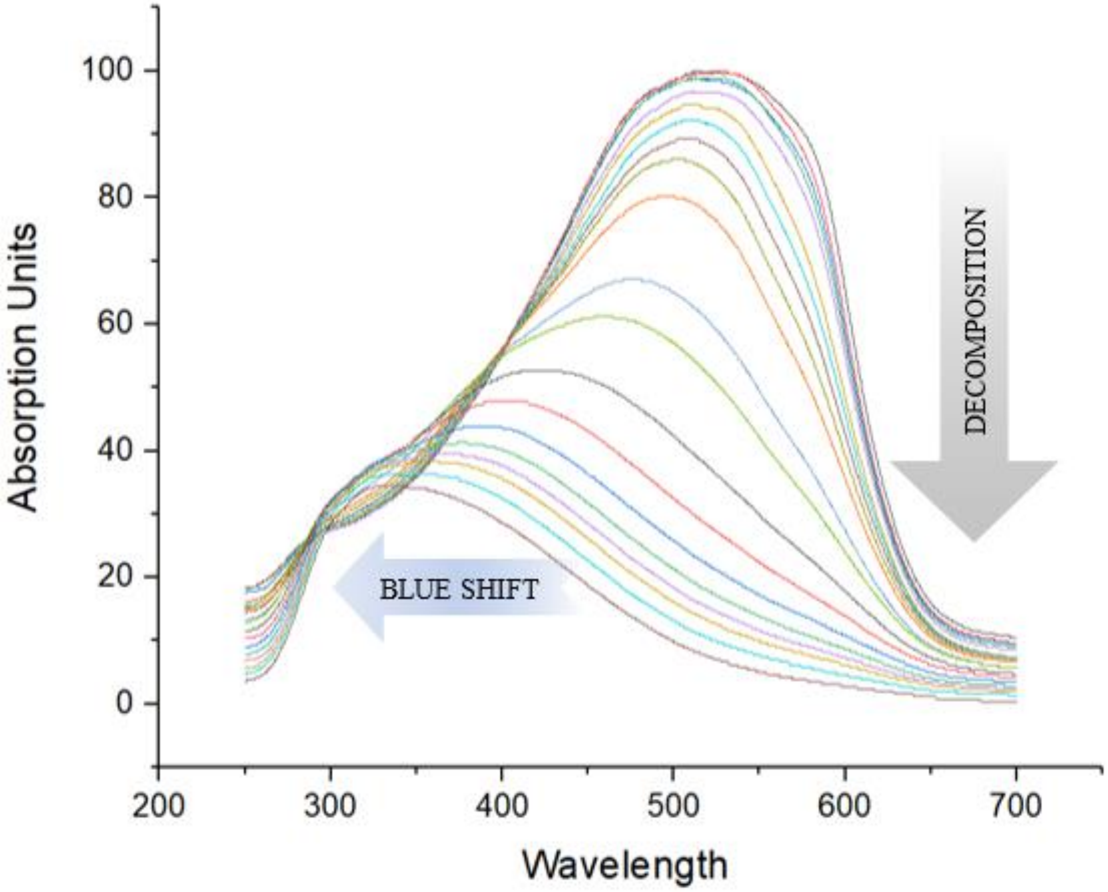

**Figure 36: Absorption spectrum of P3HT film exposed to 500 suns in air (20 min)**

Figure 36 represents the continuous absorption spectrum of a P3HT film exposed to an intensity of 500 suns under atmospheric conditions for 20 mins, data was collected every one min. As it can be clearly observed from the plot that the overall absorption decreases with time indicating the decomposition of the material and a general trend of blue shift where the peak shifts from 530nm to 320nm

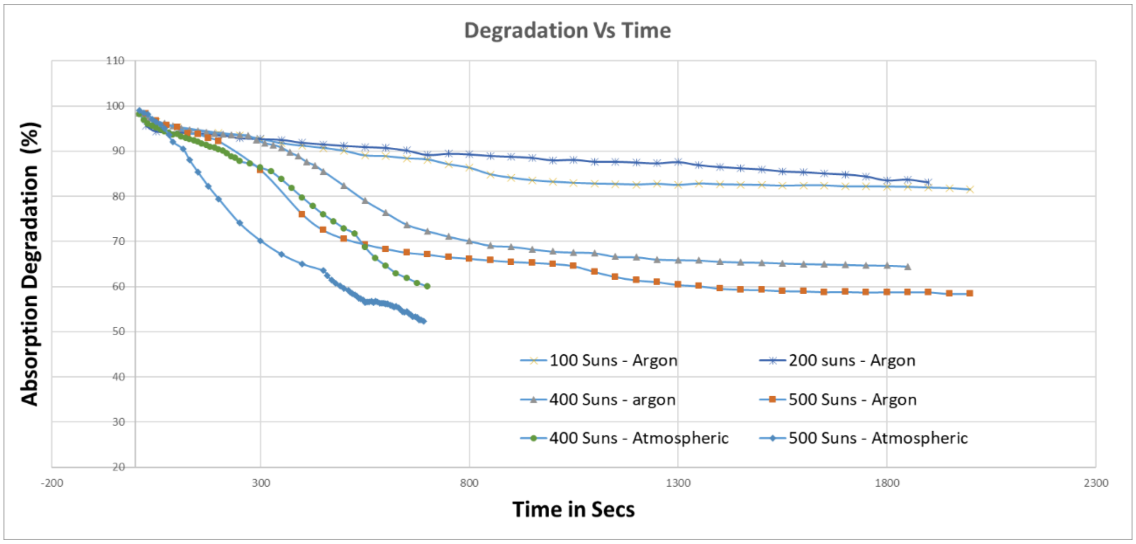

**Figure 37: Absorption degradation vs time plot for P3HT using the continuous testing methodology**

Figure 37 shows a cumulative absorption degradation vs time plot for P3HT using the continuous testing methodology. The degradation patterns while testing the lower intensities resembles a linear behavior indicating agreement with reciprocity law but as the intensity is increased to 400 and 500 suns the Schwarzschild’s equation should be used because the behavior tends to shift towards a power fit but the coefficient is still close to 1. The cumulative dosage based life time estimate for P3HT films using the continuous testing methodology is given in table 4.

**Table 4: Cumulative dosage based life time estimate for P3HT films using the continuous testing methodology**

| Environment | Time to reach 50% Degradation using the equation of the line | Minutes (± 10) | Hours | Sun*hours | Days under 1 sun (± 5) |
|---|---|---|---|---|---|
| Inert - Argon | 100 suns | 157 | 3 | 262 | 44 |
|  | 200 suns | 86 | 1 | 286 | 48 |
|  | 400 suns | 41 | 1 | 272 | 45 |
|  | 500 suns | 33 | 1 | 276 | 46 |
| Atmospheric conditions | 400 suns | 15 | 0 | 101 | 17 |
|  | 500 suns | 12 | 0 | 98 | 16 |

### 4.2.2 P3HT:PCBM

Figure 38 illustrates an overview of the degradation percentage as a function of time. The experiments were carried out in atmospheric conditions and the samples were exposed to 100, 200 and 400 suns. All the data points were repeated twice to eliminate uncertainty and error experiments. The main comparison was to analyze the effect of temperature on the absorption degradation. As it can be clearly seen that only an increase of 20$^{o}$C for even couple of minutes has a considerable effect on the overall degradation of the samples.

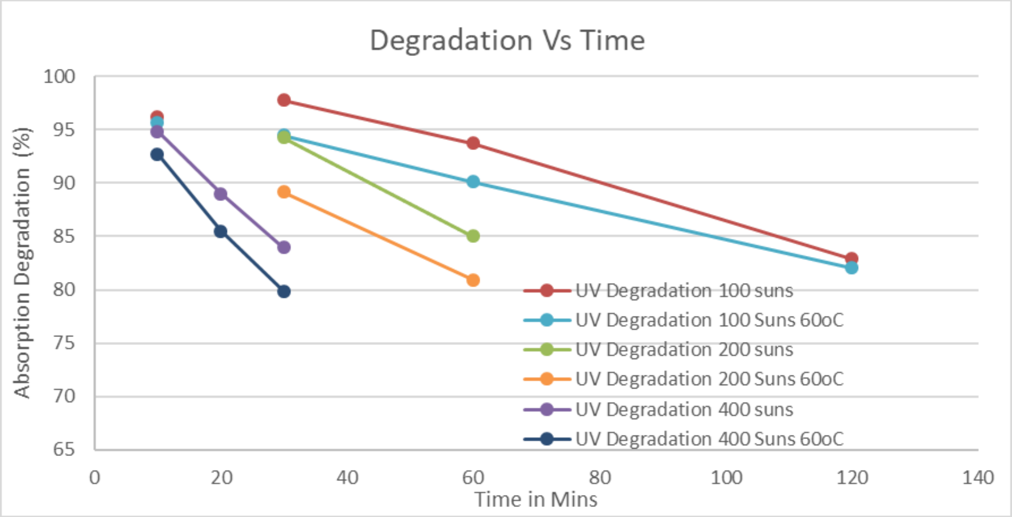

**Figure 38: Absorption degradation vs time plot for P3HT-PCBM films using the batch testing methodology for 40$^{o}$C and 60$^{o}$C.**

**Table 5: Cumulative dosage-based life time estimate for P3HT-PCBM films using the batch testing methodology under atmospheric conditions**

| Environment | Time to reach 50% Degradation using the equation of the line | Minutes (± 10) | Hours | Sun*hours | Days under 1 sun (± 5) |
|---|---|---|---|---|---|
| Atmospheric conditions | 100 suns | 375 | 6 | 626 | 104 |
| | 200 suns | 174 | 3 | 580 | 97 |
| | 400 suns | 92 | 2 | 613 | 102 |

Table 5 above summarizes the predicted lifetimes of the P3HT-PCBM films under different experimental conditions based on the cumulative dosage hypothesis (Explained in the previous sections) which converts the exposure time into sun*hours. The experiments were carried out in atmospheric conditions at 40°C. The obtained results agree with the hypothesis as the calculated number of days the sample will survive under single sun condition are very similar for different flux values and exposure times.

The UV-VIS absorption spectrum for P3HT-PCBM films exposed to 500 suns is given below. The graph illustrates the exposure time 75 mins with 5 min intervals.

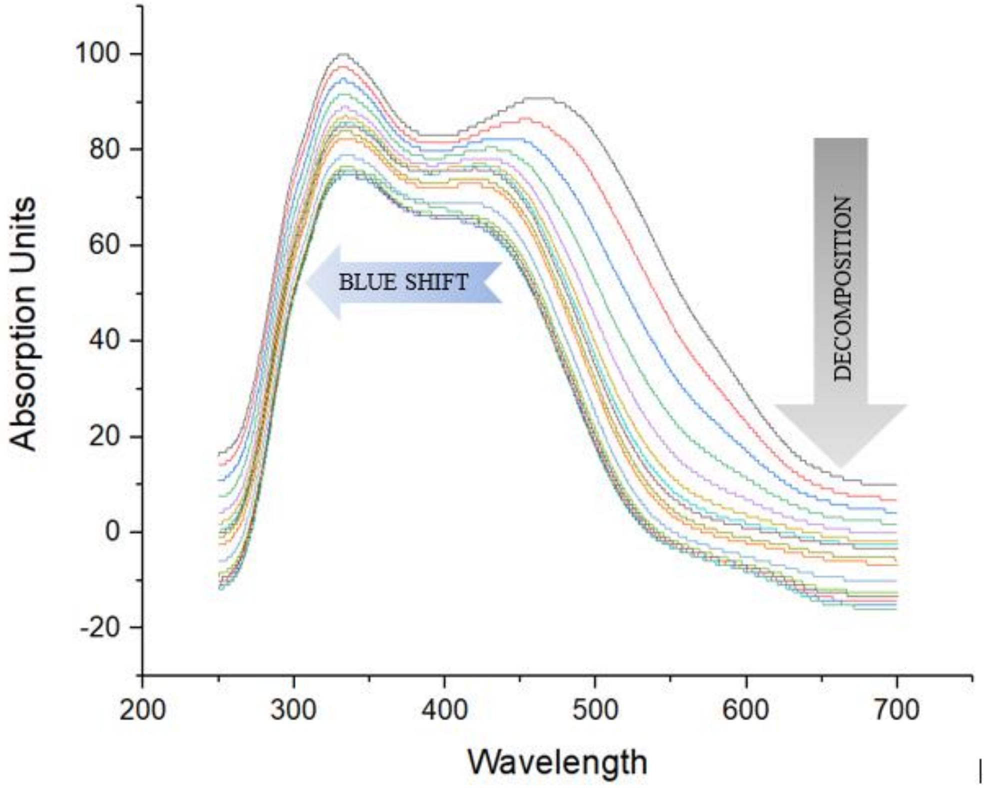

**Figure 39: P3HT- PCBM films exposed to 100 suns for 120 minutes**

As it can be seen from figure 39, the absorption spectra of P3HT-PCBM films show a blue shift indicating a higher excitation energy required by the sample. As the excitation energy is given by equation 4

$$E = hv \qquad \text{(eq. 5)}$$

Where E is the excitation energy to from a HOMO (Highest Occupied Molecular Orbital) to a LUMO (Lowest Unoccupied Molecular Orbital) state and v is the frequency. This frequency in the above equation can be substituted by restructuring the equation below;

$$c = \lambda\, v \qquad \text{(eq. 6)}$$

Where C is the speed of sound, λ is the wavelength and c is the speed of sound. The final equation correlating the excitation energy to the max wavelength is given as;

$$E = \frac{hc}{\lambda} \qquad \text{(eq. 7)}$$

### 4.3 FTIR/ATR analysis

Infrared spectroscopy of the sample mixture is obtained using the FTIR-ATR. The device can be operated either to use reflectance or transmittance to determine the absorbance or transmittance through the thin film. However, since the glass substrate absorbs a part of the Infrared range, the reflectance mode is used with the thin film facing downwards. The Attenuated Total Reflector (ATR) uses reflected infrared to determine the absorbance or transmittance through the sample [52]. As a result of the process, graphs pertaining to the absorbance or transmittance at different wavelengths are mapped. Based on the peaks observed and the intensity of peaks at different wavelengths, the bonds present in the sample are determined [53]. Each material has its own spectra that acts as a fingerprint for the material. The comparison of the spectra with literature confirms the presence of the materials and bonds observed. The material is exposed to radiation of known intensity and the ATR spectra is used to determine the probability of degradation taking place. In order to evaluate the degradation, fresh samples of P3HT-PCBM and pure P3HT are tested as the thin film on a glass substrate. The thin film is tested using a diamond crystal at a resolution of 4 cm$^{-1}$ from 650 cm$^{-1}$ to 4000 cm$^{-1}$ wavelength. The samples are exposed to different incident flux intensities and the samples are again tested under the ATR after exposure. The spectra obtained for the sample before and after exposure are compared to test the degradation. The degradation analysis using the ATR-FTIR carried out in this research is qualitative instead of quantitative.

### 4.3.1 P3HT/PCBM FTIR-ATR analysis

The P3HT-PCBM samples prepared on the glass substrate are tested in the ATR between 650 $cm^{-1}$ and 4000 $cm^{-1}$. The resultant glass with thin film is exposed to radiation of 100 suns for 1 hour (in presence of air), 200 suns for 30 minutes (in presence continuous argon flow) and 200 suns for 1 hour of static Argon environment. The exposed films are tested in the ATR at the same settings as the fresh sample. Results from FTIR-ATR are summarized below.

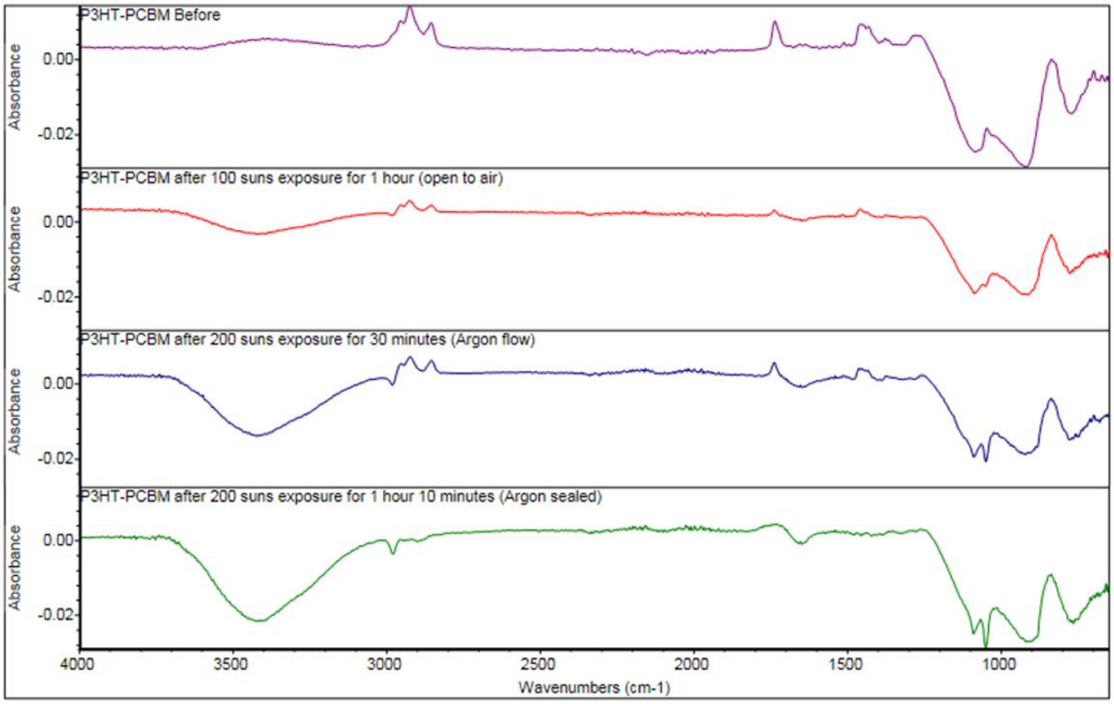

**Figure 40: ATR spectra for P3HT-PCBM fresh and aged films**

Figure 40 shows distinct spectra obtained before and after exposure. As seen from the graphs, peaks at around 2852 $cm^{-1}$ and 2921 $cm^{-1}$ are formed. According to Rodrigues et al. [36] these peaks represent the hexyl side chains. Three different peaks from 800 $cm^{-1}$ to 1200 $cm^{-1}$ are observed for the mixture. However, these peaks merge into each other not making the peaks very prominent. Peaks are observed at 1400 $cm^{-1}$ representing the presence of fullerene structure, while peaks at 1200$cm^{-1}$, 1450 $cm^{-1}$ and 1700 $cm^{-1}$ represent C-O, C=C and C=O bonds respectively [54, 55]. The peak at 800 signifies the thiophene rings [36]. The peaks formed at different wavelength are representative of the mixture of PCBM and P3HT. The peaks at 2852 $cm^{-1}$, 2921 $cm^{-1}$, 1450 $cm^{-1}$, and 800-1200 $cm^{-1}$ are representative of P3HT, while peaks at 1200 $cm^{-1}$, 1400 $cm^{-1}$, 1700 $cm^{-1}$ and 700 $cm^{-1}$ are representative of PCBM as seen in the figure 41 below.

The different spectra's are compared on the same scale, indicating the disappearance of peaks faster in presence of air as compared to inert Argon environment. Presence of air in the system leads to oxidation of the sample which causes the bonds to break faster than the inert environment. However, the peaks at 2852 $cm^{-1}$ and 2921 $cm^{-1}$ decrease in intensity, almost disappearing which could correspond to the volatilization of the hexyl chains due to exposure to radiation. The peaks seen at 1200 $cm^{-1}$, 1400 $cm^{-1}$, 1450 $cm^{-1}$ and 1700 $cm^{-1}$ tend to decrease in intensity as compared to the sample spectra before exposure. In presence of an argon atmosphere, high amount of radiation and time is required to achieve the same amount of degradation caused by air under 200 suns in 30 minutes, hence the sample sustains less photo-degradation.

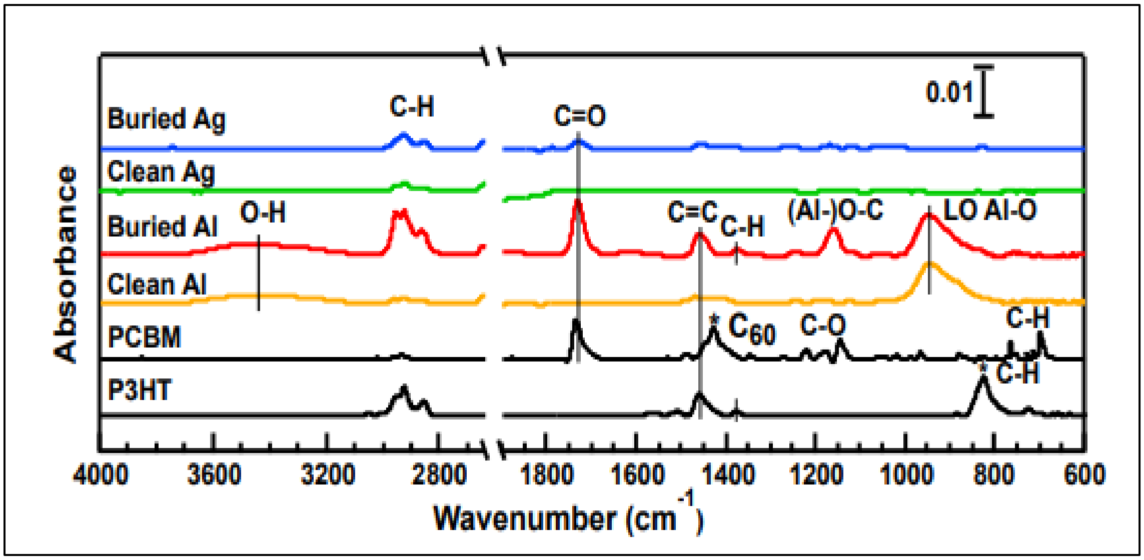

**Figure 41: Reference ATR results of PCBM and P3HT for comparison of current results, adapted from Wang et al. [56].**

### 4.3.2 P3HT FTIR-ATR analysis

P3HT is more susceptible to degradation in presence of radiation as most of the peaks representing P3HT decrease in intensity faster than the PCBM peaks as seen from the spectra figure 40 and 42. Therefore the behavior of pure P3HT exposed to radiation at different times and intensities is observed. A thin layer of pure P3HT was coated on a glass substrate and tested for reflectance in the ATR. The sample is exposed to radiation of 200 suns in presence of air, and in absence of air (Argon). The degradation time increases as the environment is switched from air to Argon as in absence of air, oxidation of sample is much lower. The sample is also tested at exposure conditions of 400 suns of flux in presence of argon and the results are depicted in figure 42.

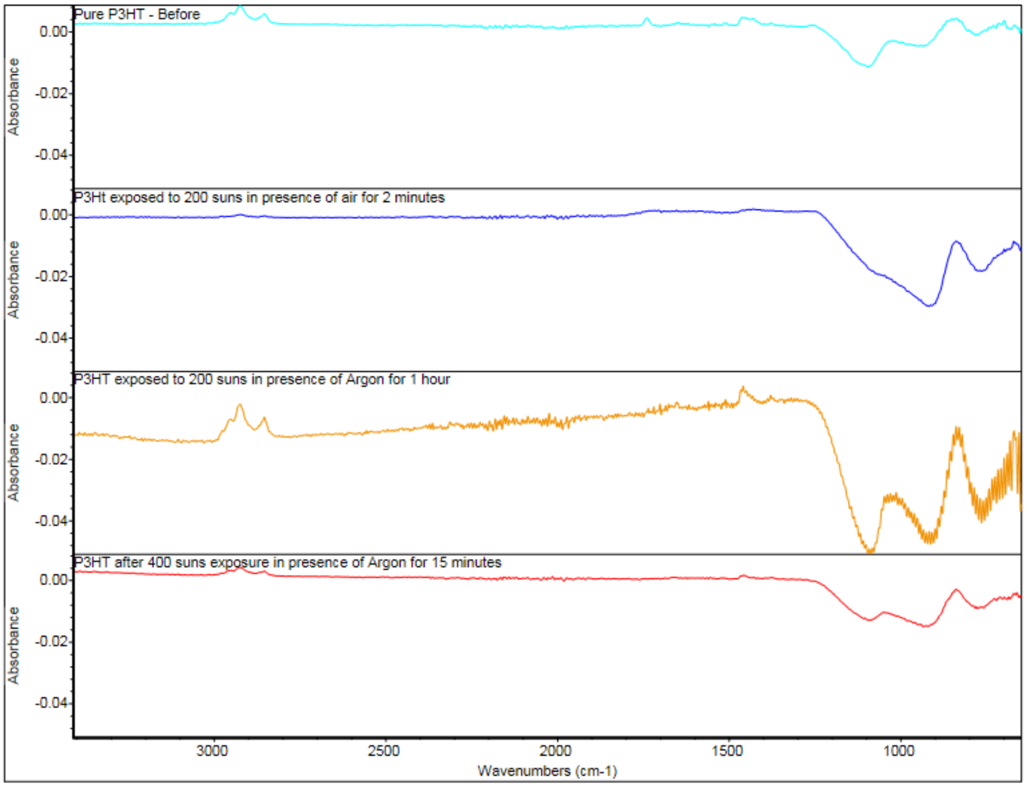

**Figure 42: ATR spectra for pure P3HT under different exposure conditions.**

As seen from figure 42, peaks formed of P3HT at 2852 cm$^{-1}$, 2921 cm$^{-1}$, 1450 cm$^{-1}$ and 1200 cm$^{-1}$ decrease in intensity within 2 minutes, when the sample is exposed to radiation of 200 suns in presence of air. However, while exposing the sample to 200 suns of radiation in an inert environment with Argon, the bonds present in P3HT break slowly as compared to samples exposed to air. Therefore, the presence of air causes oxidation of sample that speeds up the degradation of the sample. Peaks are observed between 800 cm$^{-1}$ and 1200 cm$^{-1}$ as well. However, the peaks formed at 1500 cm$^{-1}$ and 1700 cm$^{-1}$ are not clear enough due to the noise produced by the equipment. This noise corresponds to improper contact of the sample with the diamond crystal. The contact pressure increase of the sample with diamond crystal leads to cracking of the glass, hence, the contact pressure is not increased.

## 4.4 XRD analysis

X-ray diffraction (XRD) helps answer questions about the crystalline structure of objects at atomic scale. Along with it other material properties can also be obtained from XRD for example chemical composition, inter-planar spacing, strain due to deformation, preferred orientation and layer thickness [57].

The main diffraction peaks for the P3HT-based films were found to be around $2\theta^{o} = 5.49 \pm 0.07$ which are correlated with the inter-chain arrangement in P3HT linked with the interdigitated alkyl chains[58]. Another visible peak was also observed around $2\theta^{o}=10.81 \pm 0.11$ which could be related to the so-called lamellar stacking of P3HT backbones [59]; this could indicate a higher crystallinity of P3HT, which is favorable when the delocalized states are oriented in the transport direction. The material was tested when freshly prepared and then after exposure to 100 suns for 30 minutes under an inert atmosphere, the results obtained align with literature [60].

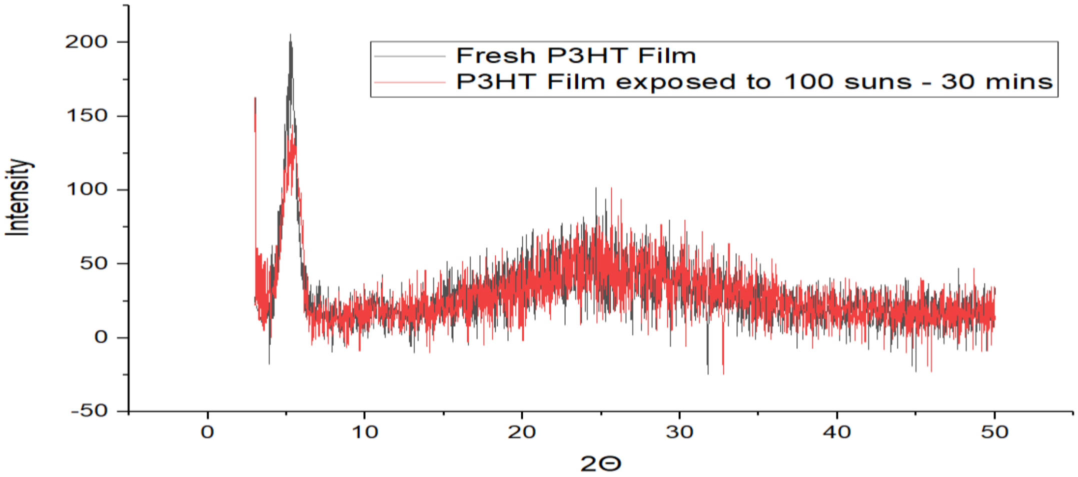

**Figure 43: XRD pattern for P3HT-PCBM fresh and aged film**

The main diffraction peak lowered and broadened in intensity compared to the original peak of the fresh sample shown in figure 43. This indicate the sample changing from a crystalline to a more amorphous structure. More tests need to be conducted to verify this hypothesis because these results are not conclusive, further testing was not conducted due to the main focus of the research being the apparatus/facility and the methodology as opposed to the materials.

### 4.5 SEM analysis

SEM analysis was conducted to visualize and compare the defects produced in the surface of the P3HT-PCBM films. The main idea of the analysis is to compare the samples exposed to concentrated light under an inert atmosphere and under atmospheric conditions [61]. The SEM images for the fresh unexposed samples are illustrated in section 4.1. The surface of the P3HT-PCBM film exposed to 200 suns at atmospheric conditions suffered from surface cracking localized to the main concentrated area of exposure with micro-cracks being developed throughout the sample (Figure 44). The images below were captured at 500, 1000, 10,000 and 20,000x magnifications. The samples exposed to 200 suns at inert conditions suffered from considerably less cracking as it can be clearly seen in Figure 45. There are no micro-cracks that are visible in the surface of these samples which account to the different atmospheric conditions of the experiment. The results show the impact of the testing the OPV materials in inert material compared to atmospheric conditions. Hence to have realistic results that replicate real world performance, it is necessary that the materials are tested in a controlled environment and that's where the apparatus designed in this research substantial.

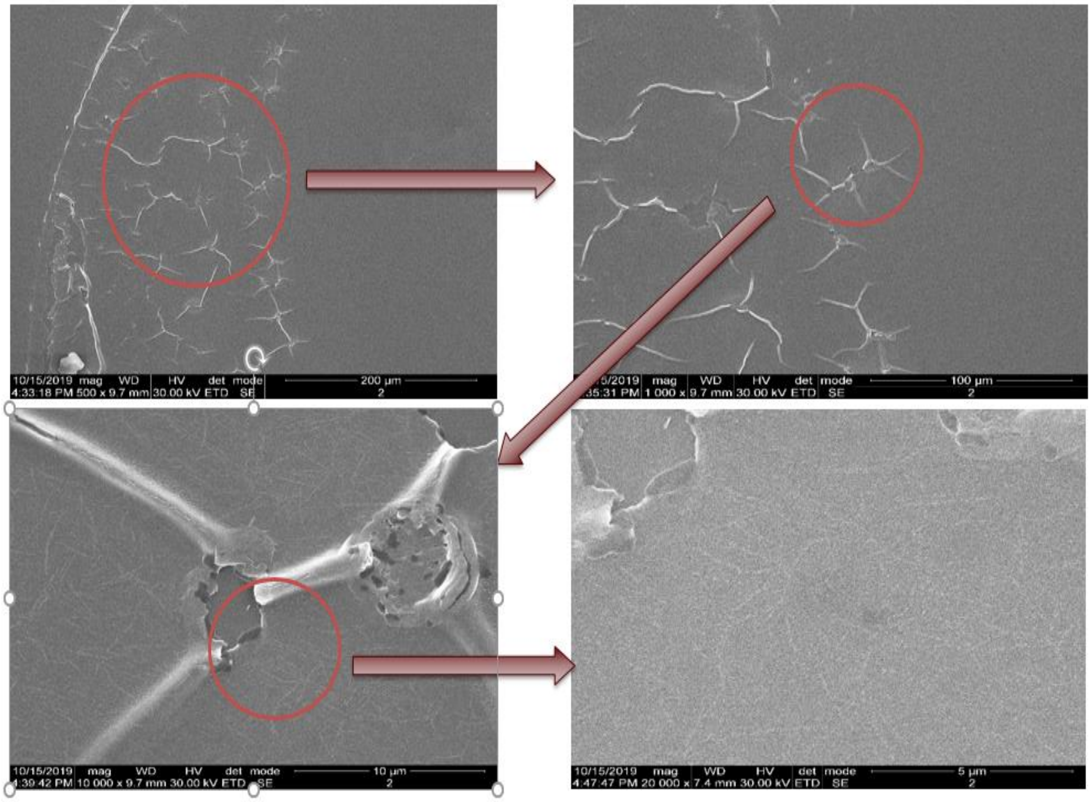

**Figure 44: Micro-cracking at the surface of P3HT-PCBM films exposed to 200 suns at atmospheric condition**

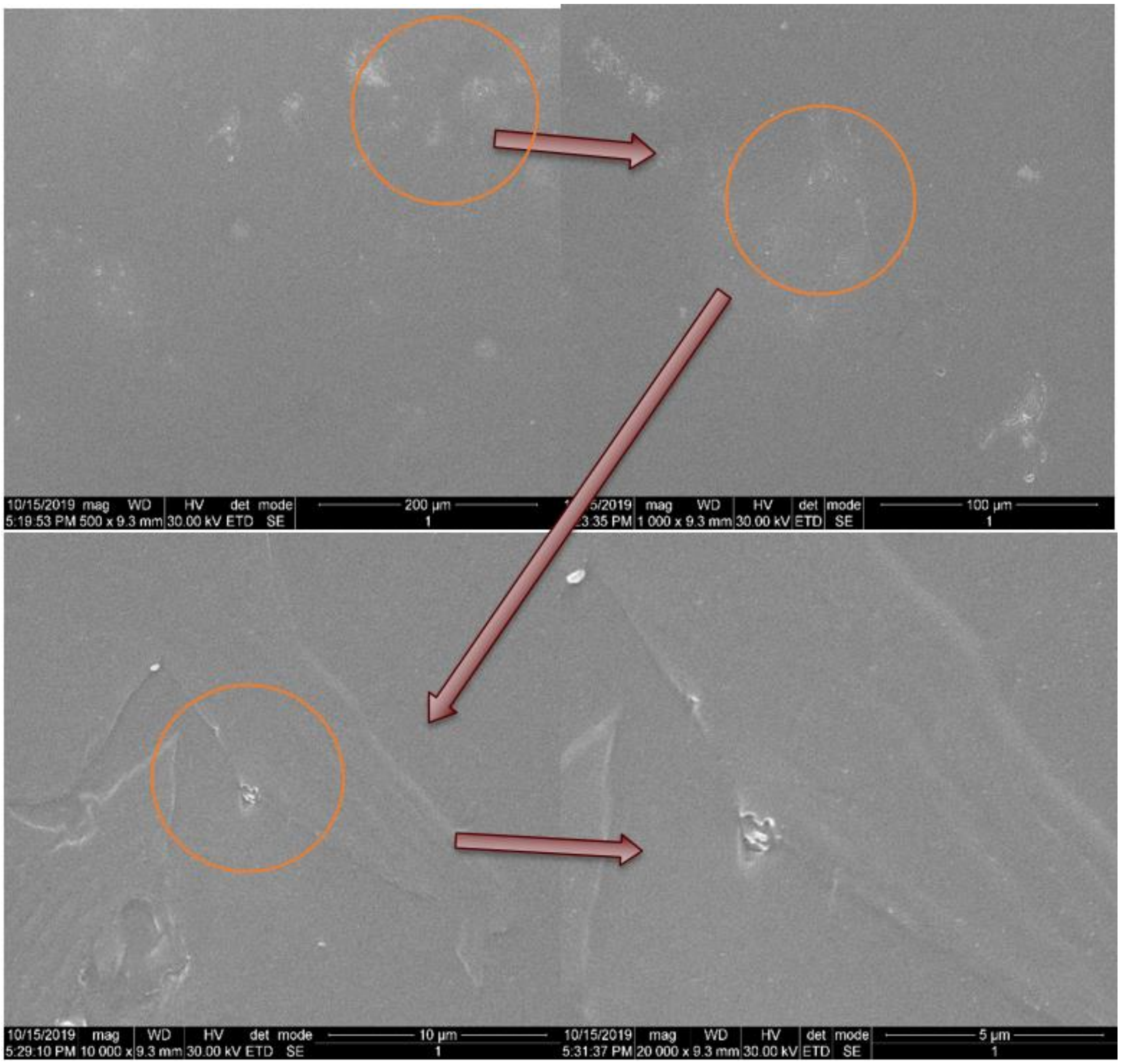

**Figure 45: Surface of P3HT-PCBM films exposed to 200 suns in an inert environment.**

## 4.6 Photo-degradation analysis using reciprocity law

### 4.6.1 P3HT-PCBM exposed to different flux values at 40°C in atmospheric conditions

The P3HT-PCBM samples are exposed at 100, 200 and 400 suns. The data obtained is extrapolated is used to measure the time taken for 50% degradation of the material. As the reciprocity law with the Schwarzschild modification is given by equation 1. By taking the natural logarithm on both the sides of the equation, converts it into the equation of a straight line.

$$I^p t = constant \qquad \text{(eq. 8)}$$

$$\ln(t) = \ln(k) - \mathrm{p}\ln(I) \qquad \text{(eq. 9)}$$

Where, k is the constant corresponding to equation 1. Since, the data collected at 100 suns and 400 suns is used to predict the time taken for 50% degradation, these are used as the two points to fit equation 3. Plotting natural logarithm of time, ln (t) v/s natural logarithm of intensity, ln (I) gives the value of p as the negative slope of the graph and ln (k) as the intercept of the graph.

As shown in figure 46, a plot of ln (t) v/s ln (I) is linear in nature with a negative slope. The slope sets value of p for 50% degradation of P3HT-PCBM to be 1.0147. The intercept is found to be 6.4849. However, to verify that the value of p remains constant with respect to the flux it is exposed to, the experimental results of time taken for 50% degradation at 200 suns is added to the graph.

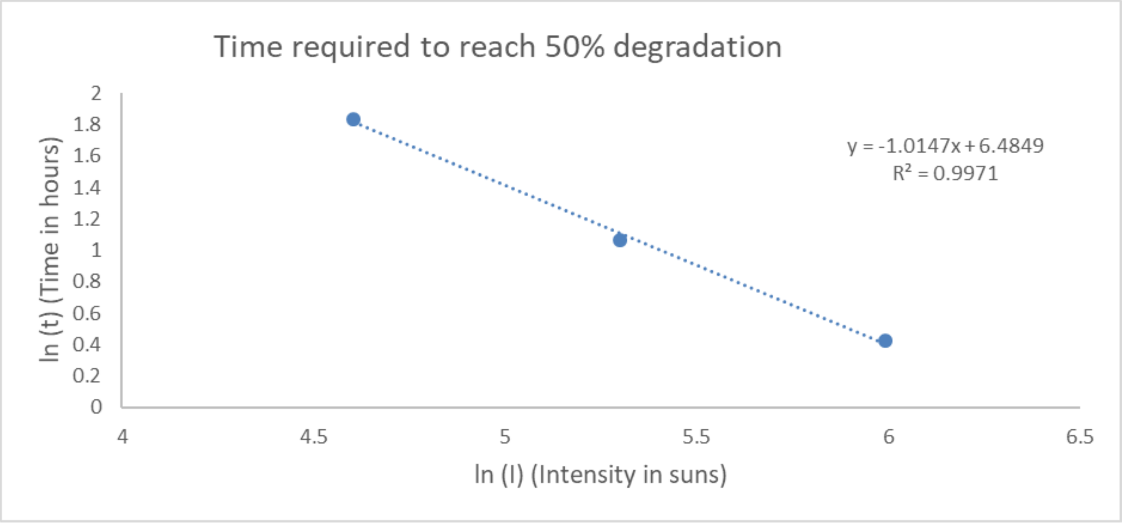

**Figure 46: Curve fitting of equation 3 with three 50% degradation data points at 40$^{o}$C**

According to figure 46, the data point corresponding to 200 suns lies on the straight line formed by the two data points previously. Hence, the material under study follows equation 3 with a constant value of p. That is, the value of p is independent of the incident flux and so can be generalized for the material being exposed at different radiations. The consistency of results gives the scope of applying the already established model for degradation time and intensity and the experimental data is in agreement with each other. According to Martin et al, fitting of data according to equation 8, helps generalize the results. Deviation of data from the graph in figure 46 would lead to varying values of p throughout the material [37]. However, since the data fits equation 9 efficiently, it therefore, it is assumed that the value of p remains constant throughout the material. Hence the general equation for P3HT-PCBM degradation to 50% is given as,

$$I^{1.0147}t = 655 \qquad \text{(eq. 10)}$$

Where, p = 1.0147 and k = 655

And if the value of the of 1 sun intensity is plugged into equation 4, we get the following results with the material being able to survive 110 days under atmospheric conditions if the KPI selected is overall absorption degradation and the cut off for failure is 50%. The lifetime predicted for a single sun exposure in given in table 6.

**Table 6: Lifetime predicted for a single sun exposure**

| Intensity (I) | Time (hours) | Time (days) |
|---|---|---|
| 1 | 655 | 110 |

### 4.6.2 P3HT-PCBM exposed to different flux values at 60°C in atmospheric conditions

Repeating the same methodology as in 4.6.1, the P3HT-PCBM sample exposed at 100, 200 and 400 suns at 60°C and the Graphs were extrapolated to calculate the time taken for 50% degradation given in figure 47. Modifying equation 1 by taking the natural logarithm on both the sides of the equation, converts it into the equation of a straight line.

$$\ln(t) = \ln(k) - \mathrm{p}\ln(I) \qquad \text{(eq. 11)}$$

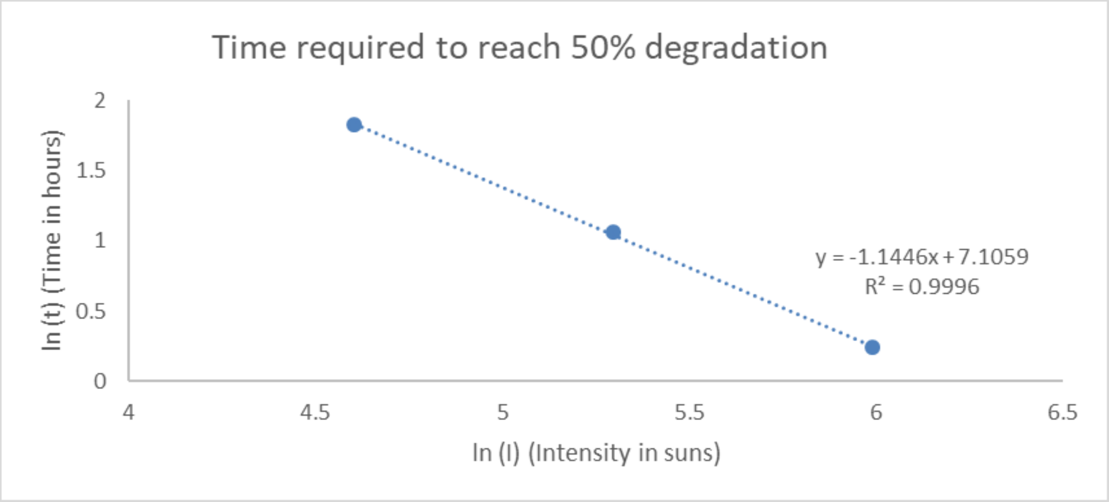

**Figure 47: Curve fitting of equation 3 with three 50% degradation data points at 60°C**

Hence the general equation for P3HT-PCBM degradation to 50% at 60°C is given as the following in eq 12 and eq 13.

$$I^{p}t = constant \qquad \text{(eq. 12)}$$

$$I^{1.1446}t = 1219.139 \qquad \text{(eq. 13)}$$

Where, p = 1.1446 and k = 1219

According to Avenel et al, the values of p vary from 0.5-1.2 as summarized by different literature studies [40]. With general equation 4, the time taken for degradation of the material (in hours) can be calculated for the given intensity (in suns) based on the reciprocity law. The constant was calculated in hours and hence the equation can be solved to calculate the value of time if the intensity value of 1 is used.

Martin et al showed that for polymeric materials the reciprocity law was obeyed in almost all cases and the distribution of the –p-coefficient used in the Schwarzschild equation is given by the following figure 48 [37].

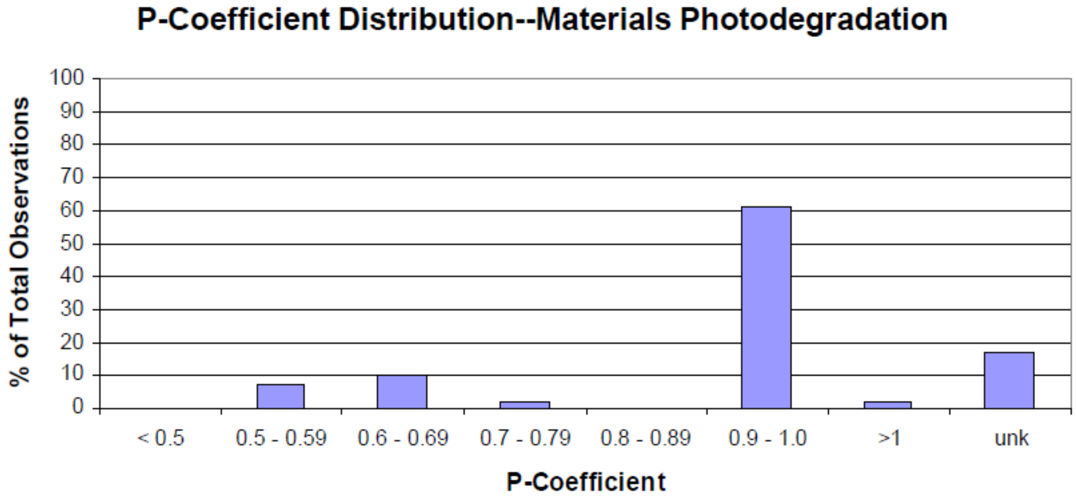

**Figure 48: P-Coefficient distribution for photo-degradation of polymers, reprinted from [37]**

# 5. CONCLUSION AND RECOMMENDATIONS

There are limitations in the current testing methodology of solar energy materials during their early development stages. The results and findings of this research provided evidence to support the hypothesis that light induced degradation plays an important role in the overall degradation of the solar energy materials, by testing OPV materials at different experimental conditions. A novel flux characterization code and methodology that aids in a semi-automatic characterization of any light source was developed and tested. This resulted in the Commissioning of a unique solar characterization facility to conduct aging studies which can identify and quantify the photo-degradation, thermal-degradation or a combination of both. The characterization is able to generate flux distribution maps from a given image and generate contour plots.

A photo-thermal cell was designed, fabricated and tested using OPV polymer films. The solar characterization facility combined with the photo thermal cell provided an improved alternative solution to the aging facilities currently available in the market. The reactor satisfied the original hypothesis that different experimental parameters have a distinct effect on the degradation or the performance of a material and to accurately conduct accelerated aging testing on the samples, the samples must be tested where the effect of all the parameters are taken into account simultaneously. The cell also provided a setup where the performance degradation of a sample can be measured on line (continuously) instead of a batch process. This reduced experimental time and also any human error caused by the handling of the sample in between the samples. This study also proved the concept of the cell by testing several reference with applications in organic photovoltaics. More specifically, samples of pure P3HT and blends of P3HT and PCBM were tested under different experimental conditions.

The observations from testing the OPV films resulted in the validation of the effective dosage hypothesis presented in the reciprocity law. At lower concentrations, there was a linear relationship and materials followed reciprocity law but however, as the intensity was increased to 400-500 suns, the Schwarzschild’s modification had be taken into account and the P-coefficient increased from 1.04 to 1.12 for the experiments carried out using the batch method.

## 5.1 Recommendations and future work

The current apparatus and the methodology requires the flux to be measured using a heat flux gage and then replace that flux gage with the cell and align it using optical accessories to be in the exact same spatial location. This may increase the uncertainty in the results due to human error. To overcome this shortcoming, a supplementary experimental support frame should be designed and fabricated to increase the accuracy and eliminate the human error that may occur. This support should be fixed in place and should be able to accommodate both the flux gage and the cell. It should incorporate a sliding mechanism with the optical accessories to increase precision.

The apparatus and the methodology developed under this project is planned to be offered as a service to the technical, industrial and scientific communities via our current facilities at TAMUQ initially. This service can further be expanded as a global service. The apparatus and auxiliary equipment can also be marketed as a solar aging compact unit by founding a small start-up company.

# REFERENCES

1. UN. (2016). "The Paris Agreement." Retrieved Dec 2018, from http://unfccc.int/paris_agreement/items/9485.php.
2. IEA. (2016). "World Energy Outlook 2016." Retrieved Dec 2018, from http://www.iea.org/newsroom/news/2016/november/world-energy-outlook-2016.html.
3. UN. (2015). "Energy Statistics Yearbook ", from https://unstats.un.org/unsd/energy/yearbook/default.htm.
4. IRENA. (2016). "Renewable Energy Statistics 2016." from http://www.irena.org/DocumentDownloads/Publications/IRENA_RE_Capacity_Statistics_2016.pdf.
5. IRENA. (2017). "Renewable Capacity Statistics 2017." from http://www.irena.org/DocumentDownloads/Publications/RE_stats_highlights_2017.pdf.
6. Vaughan, A. *Time to shine: Solar power is fastest-growing source of new energy*. (2017)Retrieved from https://www.theguardian.com/environment/2017/oct/04/solar-power-renewables-international-energy-agency
7. *U.S. Energy Information Administration - EIA - Independent Statistics and Analysis. (2013, July 25). Retrieved from https://www.eia.gov/todayinenergy/detail.php?id=12251#*.

8. Laing, D., et al., *Economic Analysis and Life Cycle Assessment of Concrete Thermal Energy Storage for Parabolic Trough Power Plants.* Journal of Solar Energy Engineering, 2010. **132**(4).

9. García-Segura, A., et al., *Durability studies of solar reflectors: A review.* Renewable and Sustainable Energy Reviews, 2016. **62**: p. 453-467.

10. Boubault, A., et al., *Aging of solar absorber materials under highly concentrated solar fluxes.* Solar Energy Materials and Solar Cells, 2014. **123**: p. 211-219.

11. Hartzell, A.L., M.G. da Silva, and H.R. Shea, *Lifetime Prediction*, in *MEMS Reliability*. 2011. p. 9-42.

12. Köhl, M., et al., *Advanced procedure for the assessment of the lifetime of solar absorber coatings.* Solar Energy Materials and Solar Cells, 2004. **84**(1-4): p. 275-289.

13. Núñez, N., et al., *Novel accelerated testing method for III–V concentrator solar cells.* Microelectronics Reliability, 2010. **50**(9-11): p. 1880-1883.

14. Boubault, A., et al., *Accelerated Aging of a Solar Absorber Material Subjected to Highly Concentrated Solar Flux.* Energy Procedia, 2014. **49**: p. 1673-1681.

15. Escobar, L.A. and W.Q. Meeker, *A Review of Accelerated Test Models.* Statistical Science, 2006. **21**(4): p. 552-577.

16. Köhl, M., et al., *Durability of polymeric glazing materials for solar applications.* Solar Energy, 2005. **79**(6): p. 618-623.

17. Guiheneuf, V., et al., *Effects of the irradiance intensity during UV accelerated aging test on unencapsulated silicon solar cells.* Solar Energy, 2017. **157**: p. 477-485.

18. Tromholt, T., et al., *Effects of concentrated sunlight on organic photovoltaics.* Applied Physics Letters, 2010. **96**(7).

19. Katz, E., et al., *Accelerated stability testing of organic photovoltaics using concentrated sunlight*. 2012. 003249-003252.

20. Cotfas, D.T., et al., *Accelerated Life Test for Photovoltaic Cells Using Concentrated Light.* International Journal of Photoenergy, 2016. **2016**: p. 1-7.

21. Sarwar, J., et al., *Description and characterization of an adjustable flux solar simulator for solar thermal, thermochemical and photovoltaic applications.* Solar Energy, 2014. **100**: p. 179-194.

22. Keck, T., et al., *EuroDish – an innovative dish/Stirling system*. 2002.

23. Gallo, A., et al., *High flux solar simulators for concentrated solar thermal research: A review.* Renewable and Sustainable Energy Reviews, 2017. **77**: p. 1385-1402.

24. Codd, D., et al., *A low cost high flux solar simulator.* Solar Energy - SOLAR ENERG, 2010. **84**: p. 2202-2212.

25. Meng, Q., Y. Wang, and L. Zhang*, Irradiance characteristics and optimization design of a large-scale solar simulator.* Solar Energy - SOLAR ENERG, 2011. **85**: p. 1758-1767.

26. Petrasch, J.r., et al., *A Novel 50 kW 11,000 suns High-Flux Solar Simulator Based on an Array of Xenon Arc Lamps.* Journal of Solar Energy Engineering, 2007. **129**(4).

27. Neumann, A. and U. Groer, *Experimenting with concentrated sunlight using the DLR solar furnace.* Solar Energy, 1996. **58**(4): p. 181-190.

28. Leveque, G., et al., *Experimental and numerical characterization of a new 45 kW_el multisource high-flux solar simulator.* Optics Express, 2016. **24**: p. A1360.

29. Tsoi, W.C., et al., *Effects of a Heavy Atom on Molecular Order and Morphology in Conjugated Polymer:Fullerene Photovoltaic Blend Thin Films and Devices.* ACS Nano, 2012. **6**(11): p. 9646-9656.

30. Heeney, M., et al., *Regioregular poly(3-hexyl)selenophene: a low band gap organic hole transporting polymer.* Chem Commun (Camb), 2007(47): p. 5061-3.

31. Wirix, M.J.M., et al., *Three-Dimensional Structure of P3HT Assemblies in Organic Solvents Revealed by Cryo-TEM.* Nano Letters, 2014. **14**(4): p. 2033-2038.

32. Holliday, S., et al., *High-efficiency and air-stable P3HT-based polymer solar cells with a new non-fullerene acceptor.* Nature Communications, 2016. **7**: p. 11585.

33. Wang, Y., et al., *Controlling morphology and crystalline structure in poly(3-hexylselenophene) solutions during aging.* RSC Adv., 2015. **5**(130): p. 107970-107976.

34. Alghamdi, A.A.B., et al., *Selenophene vs. thiophene in benzothiadiazole-based low energy gap donor–acceptor polymers for photovoltaic applications.* Journal of Materials Chemistry A, 2013. **1**(16).

35. Hrostea, L., et al., *Optical and Morphological Properties of P3HT and P3HT: PCBM Thin Films Used in Photovoltaic Applications.* IOP Conference Series: Materials Science and Engineering, 2018. **374**: p. 012015.

36. Rodrigues, A., et al., *Thermal stability of P3HT and P3HT:PCBM blends in the molten state.* Polymer Testing, 2013. **32**(7): p. 1192-1201.

37. Martin, J.W., J.W. Chin, and T. Nguyen, *Reciprocity law experiments in polymeric photodegradation: a critical review.* Progress in Organic Coatings, 2003. **47**(3): p. 292-311.

38. Claesson, S., L. Juhlin, and G. Wettermark, *The reciprocity law of Uv-irradiation effects; damage on mouse skin exposed to Uv-light varied over a 107-fold intensity range.* Acta Derm Venereol, 1958. **38**(2): p. 123-36.

39. Crewdson, L. and K. Scott, *A Comparison of Experimental High Irradiance and Standard SAE Weathering Tests for Automotive Exterior Materials.* SAE Transactions, 1994. **103**: p. 621-628.

40. Avenel, C., et al., *Review of accelerated ageing test modelling and its application to solar mirrors.* Solar Energy Materials and Solar Cells, 2018. **186**: p. 29-41.

41. Bunsen, R. and H. Roscoe, *Photochemische Untersuchungen.* Annalen der Physik, 2006. **184**: p. 193-273.

42. *ASTM International. G169-01(2013) Standard Guide for Application of Basic Statistical Methods to Weathering Tests. West Conshohocken, PA; ASTM International, 2013. doi: https://doi.org/10.1520/G0169-01R13.*

43. *ASTM International. G141-09(2013) Standard Guide for Addressing Variability in Exposure Testing of Nonmetallic Materials. West Conshohocken, PA; ASTM International, 2013. doi: https://doi.org/10.1520/G0141-09R13.*

44. *ASTM International. G172-19 Standard Guide for Statistical Analysis of Accelerated Service Life Data. West Conshohocken, PA; ASTM International, 2019. doi: https://doi.org/10.1520/G0172-19.*

45. Hintz, H., et al., *Photodegradation of P3HT−A Systematic Study of Environmental Factors.* Chemistry of Materials, 2011. **23**(2): p. 145-154.

46. *Thin Film Coating Solution-Processing Techniques Compared. (n.d.). Retrieved from https://www.ossila.com/pages/solution-processing-techniques-comparison#DoctorBlading.*

47. *Spin Coating: Complete Guide to Theory and Techniques. (n.d.). Retrieved from https://www.ossila.com/pages/spin-coating*

48. *Eslamian, M., & Zabihi, F. (2015). Ultrasonic Substrate Vibration-Assisted Drop Casting (SVADC) for the Fabrication of Photovoltaic Solar Cell Arrays and Thin-Film Devices. Nanoscale Research Letters.*

49. *Thin Film Coating Solution-Processing Techniques Compared. (n.d.). Retrieved from https://www.ossila.com/pages/solution-processing-techniques-comparison#DipCoating.*

50. Bag, M., et al., *Fabrication Conditions for Efficient Organic Photovoltaic Cells from Aqueous Dispersions of Nanoparticles.* RSC Advances, 2014. **4**: p. 45325-45331.

51. De Caro, C. and C. Haller, *UV/VIS Spectrophotometry - Fundamentals and Applications*. 2015.

52. Grdadolnik, J., *ATR-FTIR spectroscopy: Its advantages and limitations.* Acta Chimica Slovenica, 2002. **49**: p. 631-642.

53. Rytwo, G., R. Zakai, and B. Wicklein, *The Use of ATR-FTIR Spectroscopy for Quantification of Adsorbed Compounds.* Journal of Spectroscopy, 2015. **2015**: p. 8 pp.

54. Thompson, L.D., *Understanding Polymers in Thin Films to Improve Photovoltaic Properties and Surface Bound Polymerization.* 2014.

55. Mahato, S., et al., *Studies on the Interaction and Complexation of Pyrrole Compound with Hemoglobin.* Journal- Indian Chemical Society, 2017. **94**: p. 949-958.

56. Wang, J., et al., *Effect of metal/bulk-heterojunction interfacial properties on organic photovoltaic device performance.* J. Mater. Chem. A, 2014. **2**.

57. Jeffery, G.A., *Elements of x-ray diffraction (Cullity, B. D.).* Journal of Chemical Education, 1957. **34**(4): p. A178.

58. Brown, P., et al., *Effect of interchain interactions on the absorption and emission of poly(3-hexylthiophene).* Physical Review B, 2003. **67**: p. 064203.

59. Brinkmann, M. and J.C. Wittmann, *Orientation of Regioregular Poly(3-hexylthiophene) by Directional Solidification: A Simple Method to Reveal the Semicrystalline Structure of a Conjugated Polymer.* Advanced Materials, 2006. **18**(7): p. 860-863.

60. Molefe, F., et al., *Spectroscopic investigation of charge and energy transfer in P3HT/GO nanocomposite for solar cell applications.* Advanced Materials Letters, 2016. **2017**: p. 246-250.

61. Motaung, D., et al., *Investigation on the effects of substrate annealing on the properties of polymer blends*. 2015.